NASA/CR–2018-219800/Volume I

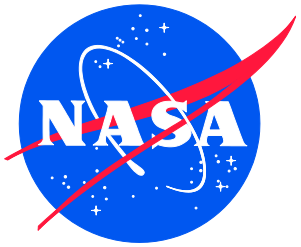

Methodologies for Verification and Validation of Space Launch System (SLS) Structural Dynamic Models

Robert N. Coppolino
Measurement Analysis Corporation, Reston, Virginia

January 2018

NASA STI Program . . . in Profile

Since its founding, NASA has been dedicated to the advancement of aeronautics and space science. The NASA scientific and technical information (STI) program plays a key part in helping NASA maintain this important role.

The NASA STI program operates under the auspices of the Agency Chief Information Officer. It collects, organizes, provides for archiving, and disseminates NASA's STI. The NASA STI program provides access to the NTRS Registered and its public interface, the NASA Technical Reports Server, thus providing one of the largest collections of aeronautical and space science STI in the world. Results are published in both non-NASA channels and by NASA in the NASA STI Report Series, which includes the following report types:

- TECHNICAL PUBLICATION. Reports of completed research or a major significant phase of research that present the results of NASA Programs and include extensive data or theoretical analysis. Includes compilations of significant scientific and technical data and information deemed to be of continuing reference value. NASA counter-part of peer-reviewed formal professional papers but has less stringent limitations on manuscript length and extent of graphic presentations.

- TECHNICAL MEMORANDUM. Scientific and technical findings that are preliminary or of specialized interest, e.g., quick release reports, working papers, and bibliographies that contain minimal annotation. Does not contain extensive analysis.

- CONTRACTOR REPORT. Scientific and technical findings by NASA-sponsored contractors and grantees.

- CONFERENCE PUBLICATION. Collected papers from scientific and technical conferences, symposia, seminars, or other meetings sponsored or co-sponsored by NASA.

- SPECIAL PUBLICATION. Scientific, technical, or historical information from NASA programs, projects, and missions, often concerned with subjects having substantial public interest.

- TECHNICAL TRANSLATION. English-language translations of foreign scientific and technical material pertinent to NASA's mission.

Specialized services also include organizing and publishing research results, distributing specialized research announcements and feeds, providing information desk and personal search support, and enabling data exchange services.

For more information about the NASA STI program, see the following:

- Access the NASA STI program home page at *http://www.sti.nasa.gov*

- E-mail your question to help@sti.nasa.gov

- Phone the NASA STI Information Desk at 757-864-9658

- Write to:
  NASA STI Information Desk
  Mail Stop 148
  NASA Langley Research Center
  Hampton, VA 23681-2199

NASA/CR–2018-219800/Volume I

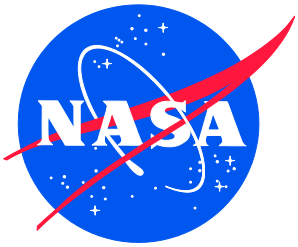

Methodologies for Verification and Validation of Space Launch System (SLS) Structural Dynamic Models

Robert N. Coppolino
Measurement Analysis Corporation, Reston, Virginia

National Aeronautics and
Space Administration

Langley Research Center
Hampton, Virginia 23681-2199

Prepared for Langley Research Center
under Contract NNL12AA09C

January 2018

Available from:

NASA Center for AeroSpace Information
7115 Standard Drive
Hanover, MD 21076-1320
443-757-5802

Table of Contents

List of Figures

List of Tables

Abstract

Responses to challenges associated with verification and validation (V&V) of Space Launch System (SLS) structural dynamics models are presented in this paper. Four methodologies addressing specific requirements for V&V are discussed. (1) Residual Mode Augmentation (RMA), which has gained acceptance by various principals in the NASA community, defines efficient and accurate FEM modal sensitivity models that are useful in test-analysis correlation and reconciliation and parametric uncertainty studies. (2) Modified Guyan Reduction (MGR) and Harmonic Reduction (HR, introduced in 1976), developed to remedy difficulties encountered with the widely used Classical Guyan Reduction (CGR) method, are presented. MGR and HR are particularly relevant for estimation of "body dominant" target modes of shell-type SLS assemblies that have numerous "body", "breathing" and local component constituents. Realities associated with configuration features and "imperfections" cause "body" and "breathing" mode characteristics to mix resulting in a lack of clarity in the understanding and correlation of FEM- and test-derived modal data. (3) Mode Consolidation (MC) is a newly introduced procedure designed to effectively "de-feature" FEM and experimental modes of detailed structural shell assemblies for unambiguous estimation of "body" dominant target modes. Finally, (4) Experimental Mode Verification (EMV) is a procedure that addresses ambiguities associated with experimental modal analysis of complex structural systems. Specifically, EMV directly separates well-defined modal data from spurious and poorly excited modal data employing newly introduced graphical and coherence metrics.

1.0 General Introduction

Verification and validation (V&V) is a highly challenging undertaking for SLS structural dynamics models due to the magnitude and complexity of SLS subassemblies and subassemblies. The following issues contribute to the overall challenge:

1. Nearly all modal testing will be conducted on non-fueled assemblies and subassemblies in the 0-60 Hz frequency band. Modes that exercise the fueled structure in this frequency band have non-fueled counterparts at natural frequencies well in excess of 60 Hz.
2. Many SLS components are configured as thin, complex construction (waffle, etc.) shell structures with attached, localized structural subassemblies (e.g., ISPE). Overall body, shell breathing, and localized subassembly dynamics in the 0-60 Hz frequency band produces a variety of technical challenges including (a) coupling of body, breathing and local kinetic energies in individual modes due to configuration features and imperfections, (b) sensitivity of shell breathing modes to static (pressure) loads, (c) sensitivity of modes to uncertainties primarily in joint stiffnesses.
3. There exist a large number of modes (~1000s for the entire SLS L/V) in the 0-60 Hz band, resulting in the following technical challenges; (d) Modal test planning and execution requires large instrumentation and excitation resources to appropriately map system modes, (e) practically achievable test-analysis correlation and reconciliation must focus on a target mode subset, which is difficult to properly select, and (f) experimental modal analysis of systems with many closely-

spaced modes requires objective quality metrics that are independent of mathematical model predictions.

This report addresses SLS structural dynamics V&V challenges by suggested employment of four methodology classes, namely:

1. **Residual Mode Augmentation (RMA)**, a technique that defines a set of "residual" trial vectors appended to baseline system modes to produce reduced-order sensitivity models that closely follow sensitivity behavior of corresponding very-large-order FEM representations. *RMA is gaining wide acceptance in our technical community as evidenced by its exercise by Dr. Eric Stewart of NASA/MSFC and Dr. Paul Blelloch of ATA.*
2. **Model Order Reduction (HR & MGR)**, alternatives to Classical Guyan Reduction (CGR) that define "body and selected dominant" shape functions based on assumed geometric shapes [Harmonic Reduction (HR)] or "load patches" rather than point loads [Modified Guyan Reduction (MGR)]. HR is a model order reduction method, formally introduced in 1976 to improve solution efficiency for propellant tank hydroelastic models. Initial motivation for MGR was the result of difficulties encountered in the past decade by Dr. Paul Blelloch during modal test planning on a structure modeled with 3-D elastic elements. *HR and MGR offer new opportunities in (a) mathematical model target mode selection and (b) experimental target mode identification. Most significantly, (c) MGR provides the "kernel" ingredient for modal consolidation.*
3. **Mode Consolidation (MC)**, a strategy for consolidation of "split" or "fragmented" modes, which used selected shape functions defined in MGR to (a) select "body dominant" system modes on the basis of kinetic energy distribution, and (b) consolidate apparently repeated "body dominant" modal fragments into idealized body modes of an apparent "de-featured" dynamic system. *MC for experimental modes combined with MGR for a system mathematical model may provide new opportunities for effective, focused test-analysis correlation and reconciliation that deliberately focus on target modes.*
4. **Experimental Mode Verification (EMV)**, an approach to test the authenticity of modes estimated via experimental modal analysis that is independent of mathematical model data (e.g., the TAM mass matrix). This approach employs the experimental mode shapes (more precisely the left-hand eigenvectors) as a transformation on measured frequency response arrays to verify the quality of experimental mode isolation. EMV is somewhat related to recent work on the SMAC algorithm by Randy Mayes of Sandia National Laboratories. *The need for a procedure such as EMV was recently indicated by difficulties encountered by NASA/MSFC during use of the B&K Reflex system for experimental analysis of ISPE measured data.*

2.0 Preliminary Comments

Before discussion of the four methodologies, key aspects of modern structural dynamic modeling practices should be noted. The following publications and reports by the writer provide details of foundational subject matters:

1. Harris' Shock and Vibration Handbook, 6th Edition, Piersol & Paez, McGraw-Hill, 2010 (Chapter 23, Finite Element Methods of Analysis)
2. "Understanding Large Order Finite Element Model Dynamic Characteristics", IMAC 29, 2011
3. "Variational Foundations of Modern Structural Dynamics", IMAC 32, 2014
4. "Structural Dynamics Modeling – Tales of Sin and Redemption", IMAC 33, 2015
5. "Launch Vehicle Propellant Tank Hydroelastic Analysis (1976-2016)", lecture at Seoul National University, ROK, October 2016 **(provided in Appendix A)**
6. "Review and Recommendations Regarding NESC-RP-14-00946, ", Note to Loads & Dynamics TDT, 5 December 2016 **(provided in Appendix B)**

The cited materials stress the significance of structural dynamic mode sensitivity to structural joint flexibilities that are often neglected in detailed finite element models. Moreover, structural dynamic damping in many structural assemblies is concentrated in those typically neglected flexible joints (damping in basic metallic structural members (e.g., rods, beams, panels, shells) is extremely low.

Natural frequencies and mode shapes of thin shell (and other structural assemblies, notably offshore jacket platforms) are ideally grouped in (a) body mode families (e.g. bending, axial, torsion and "bulge" [especially fluid-filled tanks]) and (b) breathing mode families. Breathing modes tend to occur well within the frequency band of fundamental body modes. In addition, breathing modes (especially those associated with singly curved, cylindrical regions) are strongly sensitive to static internal pressure and "weight" structural loading; in contrast, body modes tend to be insensitive to static loadings (as a general rule).

Structural features and imperfections (especially in joints) tend to produce structural modes of thin shell structures which have mixed body and breathing characteristics. This results in analytical and experimental modes that are difficult to categorize and discern. The mixed character modes often appear as repeated body modes, differing from one another merely due to the phase of breathing kinetic energy contributions.

Fluids represent roughly 80% of a fully fueled liquid propellant launch vehicle stage. Other than the fact that the role and mechanical modeling of fluids is largely a poorly understood "orphan" in structural dynamics practice, it is disconcerting that the majority of planned V&V modal tests on SLS will be conducted on dry structures in the 0-60 Hz frequency band. The empty structure fundamental axial-bulge mode will occur well above the 0-60 Hz frequency band, while the same type of fundamental mode for a fully fueled structure will certainly occur within the 0-60 Hz frequency band. This fact strongly suggests that the planned modal testing activities will not exercise some system dynamics that are significant for flight loads V&V.

Due to the complexities inherent in SLS structures, (a) thorough instrumentation and exciter resources are required to clearly map experimental system modes, and (b) mathematical models must be prepared to effectively and efficiently describe the system's parametric sensitivities. The following section summarizes an efficient strategy for treatment of parametric sensitivities.

3.0 Part 1: Residual Mode Augmentation

3.1 Introduction

Efficient computation of structural dynamic modal frequency and mode shape sensitivities associated with variation of physical stiffness and mass parameters is essential for (1) practical design sensitivity and uncertainty studies and (2) reconciliation of finite element models with modal test data. Sensitivity analysis procedures fall in two distinct categories, namely (a) modal derivatives for small parametric variation and
(b) altered system modes associated with "large" parametric variation. The latter category is generally applicable to modal testing, which often requires significant local parameter changes at joints to effect FEM-test reconciliation[1]. However, many investigators and commercial software packages employ estimated modal derivatives in optimization strategies, which address FEM-test reconciliation objectives.

Since the 1960's, methods for computation of modal frequency and mode shape derivatives have evolved. Fox and Kapoor[2] introduced an exact derivative formulation that required knowledge of all modes of the original system; application of the procedure when a truncated set of modes was employed produced compromised derivatives. In response to this difficulty, Nelson[3] derived an exact formulation for computation of mode shape derivatives for truncated mode sets. Efforts to refine and extend application of mode shape derivatives for finite parameter change sensitivity computations have been pursued by

many investigators (including the present author). However, the need for modal frequency and mode shape sensitivities that map over very large ranges for multiple parameters suggests application of alternative Ritz[4] strategies.

The Ritz method is one of the most significant developments in analytical mechanics of the past century. This method provides a logical energy formulation for consistent reduction of mass and stiffness matrices employing a set of trial vectors as a reduction transformation. Effectiveness and accuracy of the reduction process depends on selection of an appropriate trial vector set. When a truncated set of baseline system mode shapes is used as the trial vector set (popularly known as Structural Dynamic Modification (SDM)[5], the Ritz method often produces poor estimates for the altered system. Augmentation of the truncated baseline system mode shapes with appropriately defined additional vectors, however, has been found to produce extremely accurate altered system modal frequencies and mode shapes. Quasi-static residual vectors[6], appended to a truncated set of mode shapes, were found to produce extremely accurate modes for offshore oil platform models subjected to localized alterations[7]. Residual Mode Augmentation (RMA), introduced in 2002[1] and thoroughly discussed in references 8 and 9, is a procedure that defines augmented trial vectors, which are appropriate for structures subjected to highly distributed, as well as localized, alterations.

3.2 Nomenclature

Symbol	Definition
[A]	Generalized mass (trial vectors)
[COR]	Cross-orthogonality
[I]	Identity
[K]	Physical stiffness
[M]	Physical mass
[OR]	Self-orthogonality
[U]	Physical displacement
[k]	Generalized stiffness
[m]	Generalized mass
p	Structural alteration parameter
[q]	Generalized displacement

Symbol	Definition
$[\Delta K]$	Physical stiffness alteration
$[\Delta M]$	Physical mass alteration
$[\Phi]$	Modal matrix
$[\Gamma]$	Unit load allocation
$[\Psi]$	Trial vector matrix
$[\Delta k]$	Generalized stiffness alteration
$[\Delta m]$	Generalized mass alteration
$[\varphi]$	Generalized mode shape
$[\lambda]$	Eigenvalue matrix

Subscript	Definition
$[\ ]_H$	High frequency
$[\ ]_L$	Low frequency
$[\ ]_O$	Baseline system
$[\ ]_S$	"Static"
$[\ ]_R$	Residual

3.3 Sensitivity Analysis Strategies

The present discussion focuses on Ritz procedures that address structural sensitivities due to stiffness and mass alterations described by large (as opposed to small) parametric variations. Therefore formulations that address computation of eigenvalue and mode shape derivatives are not considered.

3.3.1 Exact Modal Analysis of Baseline And Altered Structures

The matrix equations describing exact free vibration of baseline and altered structures, respectively, are

$$[K_O][\Phi_O]-[M_O][\Phi_O][\lambda_O]=[0], \tag{1}$$

and

$$[K_O+p\cdot\Delta K][\Phi]-[M_O+p\cdot\Delta M][\Phi][\lambda]=[0]. \tag{2}$$

It is implicitly assumed that the stiffness and mass changes scale linearly with respect to the parameter, *p*. Therefore, changes in "beam" depth may not be directly applied, since the axial stiffness (AE) scales linearly with depth and the flexural stiffness (EI) scales as the cube of depth. The appropriate formulation for equation 2 permits linear sensitivity of "AE" and "EI" separately.

The relationship between mode shapes of the baseline and altered structures is expressed as the cross-orthogonality of orthonormal mode shape sets,

$$[COR]=[\Phi_O^T][M_O][\Phi], \tag{3}$$

where

$$[OR_O] = [\Phi_O^T][M_O][\Phi_O] = [I_O] \ , \quad [OR] = [\Phi^T][M_O][\Phi] = [I]. \tag{4}$$

3.3.2 Truncated Mode Set Approximation

The most fundamental Ritz approximation, commonly used in Structural Dynamic Modification (SDM)[5], employs a truncated set of low frequency eigenvalues as the reduction transformation described by

$$[\Phi] = [\Phi_{OL}][\varphi], \tag{5}$$

where the reduced baseline structure stiffness and mass matrices, respectively, are

$$[k_O] = [\Phi_{OL}^T K_O \Phi_{OL}] = [\lambda_{OL}] \ , \quad [m_O] = [\Phi_{OL}^T M_O \Phi_{OL}] = [I_{OL}], \tag{6}$$

the reduced stiffness and mass sensitivity matrices, respectively, are

$$[\Delta k] = [\Phi_{OL}^T \Delta K \Phi_{OL}] \ , \quad [\Delta m] = [\Phi_{OL}^T \Delta M \Phi_{OL}], \tag{7}$$

and the reduced altered structure free vibration equation is

$$[\lambda_{OL} + p \cdot \Delta k][\varphi] - [I_{OL} + p \cdot \Delta m][\varphi][\lambda] = [0]. \tag{8}$$

A well-known result of this type of trial vector reduction strategy is that the approximate altered structure eigenvalues are generally higher than results for the exact solution, and the approximate mode shapes do not closely follow the exact shapes when parametric alterations are large.

3.3.3 Residual Vector Augmentation (for Local Alterations)

The static displacements for a baseline structure subjected to unit loads (at physical degrees of freedom where the structure is to be altered) described by the columns of a load array, [Γ], are the solutions of

$$[K_O][U_S] = [\Gamma], \tag{9}$$

A low frequency modal approximation of static displacements for the above system employs the transformation,

$$[U_{SL}] = [\Phi_{OL}][q_L], \tag{10}$$

resulting in the approximate static displacements,

$$[q_L] = [\lambda_L^{-1}][\Phi_{OL}^T][\Gamma] \ , \quad [U_{SL}] = [\Phi_{OL}\lambda_L^{-1}\Phi_{OL}^T][\Gamma], \tag{11}$$

The difference between the exact and approximate static solutions defines MacNeal's[6] quasi-static residual vectors,

$$[\Psi_\rho] = [U_S] - [U_{SL}] = [K_O^{-1} - \Phi_{OL}\lambda_L^{-1}\Phi_{OL}^T][\Gamma] \equiv [\Phi_{OH}\lambda_H^{-1}\Phi_{OH}^T][\Gamma], \tag{12}$$

which have been mathematically proven to be the quasi-static displacements associated with all of the high-frequency mode shapes.

An orthonormalized set of residual vectors is defined by solution of the residual eigenvalue problem[7],

$$[k_\rho] = [\Psi_\rho^T K_O \Psi_\rho] \ , \quad [m_\rho] = [\Psi_\rho^T M_O \Psi_\rho], \tag{13}$$

$$\left[k_\rho\right]\left[\varphi_\rho\right]-\left[m_\rho\right]\left[\varphi_\rho\right]\left[\lambda_\rho\right]=\left[0\right]\ ,\quad \left[\Phi_\rho\right]=\left[\Psi_\rho\right]\left[\varphi_\rho\right]$$

The augmented trial vector set (replacing the reduction transformation of equation 5) is

$$\left[\overline{\Phi}_{OL}\right]=\left[\Phi_{OL}\quad \Phi_\rho\right]. \tag{14}$$

When structural alterations are localized, relatively few residual vectors adequately describe the content of changed system mode shapes, as demonstrated in an offshore oil platform damage sensitivity study[7]. The above described innovation loses its appeal when structural alterations are well-dispersed requiring utilization of many residual vectors.

3.3.4 Robust Strategy (for Dispersed Alterations)

When structural alterations are well-dispersed, parametric structural changes may affect many physical degrees of freedom and require a description in terms of several independent scaling parameters, "p_i". The expressions for altered stiffness and mass matrices in such a situation are

$$\left[K\right]=\left[K_O\right]+\sum_{i=1}^{N}p_i\left[\Delta K_i\right]\ ,\ \left[M\right]=\left[M_O\right]+\sum_{i=1}^{N}p_i\left[\Delta M_i\right], \tag{15}$$

The altered system free vibration matrix equation for this situation is

$$\left[K_O+\sum_{i=1}^{N}p_i\left[\Delta K_i\right]\right]\left[\Phi\right]-\left[M_O+\sum_{i=1}^{N}p_i\left[\Delta M_i\right]\right]\left[\Phi\right]\left[\lambda\right]=\left[0\right], \tag{16}$$

Note that equation 1 describes the baseline system's free vibration behavior.

3.3.5 Residual Mode Augmentation (RMA)

Definition of residual vectors associated with dispersed, independent alterations of a baseline structure, described by equation 1, is accomplished by first computing the lowest frequency mode shapes of the baseline structure (equation 5) as well as the lowest mode shapes associated with each independent alteration of the structure

$$\left[K_O+\bar{p}_i\Delta K_i\right]\left[\Phi_{iL}\right]-\left[M_O+\bar{p}_i\Delta M_i\right]\left[\Phi_{iL}\right]\left[\lambda_{iL}\right]=\left[0\right]\ \text{(for i=1,…,N)}, \tag{17}$$

The selected value of each independent scaling parameter is sufficiently large to produce a substantial change in mode shapes (with respect to the baseline structure). An initial set of trial vectors that adequately (and perhaps redundantly) encompass all potential (low frequency) altered system mode shapes is

$$\left[\Psi\right]=\left[\Phi_{1L}\quad \Phi_{2L}\quad ...\quad \Phi_{NL}\right] \tag{18}$$

This set of trial vectors is expressible as the sum of (a) a linear combination of baseline system mode shapes and (b) trial vectors (that are linearly independent of the baseline system mode shapes)

$$\left[\Psi\right]=\left[\Phi_{OL}\right]\left[COR\right]+\left[\Psi'\right] \tag{19}$$

The cross-orthogonality coefficient matrix is determined based on the following least-squares solution

$$\left[\Phi_{OL}^T M_O \Psi\right]=\left[\Phi_{OL}^T M_O \Phi_{OL}\right]\left[COR\right]+\left[\Phi_{OL}^T M_O \Psi'\right]=\left[I_{OL}\right]\left[COR\right]+\left[0\right], \tag{20}$$

where

$$[COR] = [\Phi_{OL}^T][M_O][\Psi] \tag{21}$$

$$[\Psi'] = [I_{OL} - \Phi_{OL}\Phi_{OL}^T M_O][\Psi] \tag{22}$$

The "purified" trial vector set is linearly independent of the baseline system mode shapes in a manner similar to MacNeal's residual vectors, as follows:

$$\begin{aligned}[\Psi'^T M_O \Phi_{OL}] &= [\Psi^T][I_{OL} - M_O\Phi_{OL}\Phi_{OL}^T][M_O\Phi_{OL}] = [\Psi^T][M_O\Phi_{OL} - M_O\Phi_{OL}(\Phi_{OL}^T M_O\Phi_{OL})] \equiv [0] \\ [\Psi'^T K_O \Phi_{OL}] &= [\Psi^T][I_{OL} - M_O\Phi_{OL}\Phi_{OL}^T][K_O\Phi_{OL}] = [\Psi^T][K_O\Phi_{OL} - M_O\Phi_{OL}\lambda_{OL}] \equiv [0].\end{aligned} \tag{23}$$

While the "purified" trial vector set has the above property, it includes an unnecessarily large number of vectors. An appropriate, substantially smaller set of residual vectors is identified by singular value decomposition of the generalized mass matrix

$$[A] = [\Psi'^T M_O \Psi'], \tag{24}$$

The singular value decomposition process involves solution of the eigenvalue problem,

$$[A][\varphi_\rho] = [\varphi_\rho][\lambda_\rho], \quad \lambda_{\rho 1} \geq \lambda_{\rho 2} \geq \lambda_{\rho 3} \geq \ldots\ldots \tag{25}$$

The cut-off criterion, noted below employed to define suitable reduced trial vector set, is

$$\frac{\lambda_{\rho N}}{\lambda_{\rho 1}} \leq tol = 10^{-N} \text{ (where N ~ 4 to 6 is usually adequate).} \tag{26}$$

The augmented trial vector set (replacing the reduction transformation of equation 5) is

$$[\overline{\Phi}_{OL}] = [\Phi_{OL} \quad \Psi'\varphi_\rho]. \tag{27}$$

3.3.6 Multi-Parameter Sensitivity Models

The form of the resulting Ritz, multi-parameter sensitivity model (associated with selected values of the scaling parameters) is

$$\left[k_O + \sum_{i=1}^{N} p_i[\Delta k_i]\right][\varphi] - \left[m_O + \sum_{i=1}^{N} p_i[\Delta m_i]\right][\varphi][\lambda] = [0], \tag{28}$$

where

$$\begin{aligned}&[k_O] = [\overline{\Phi}_{OL}^T K_O \overline{\Phi}_{OL}] \quad , \quad [m_O] = [\overline{\Phi}_{OL}^T M_O \overline{\Phi}_{OL}] \\ &[\Delta k_i] = [\overline{\Phi}_{OL}^T \Delta K_i \overline{\Phi}_{OL}] \quad , \quad [\Delta m_i] = [\overline{\Phi}_{OL}^T \Delta M_i \overline{\Phi}_{OL}].\end{aligned} \tag{29}$$

Recovery of mode shapes in terms of physical degrees-of-freedom is accomplished with

$$[\Phi] = [\overline{\Phi}_{OL}][\varphi] \tag{30}$$

3.3.7 RMA Solution Qualities

Since its introduction in 2001, RMA has exhibited the capability to accurately follow modal sensitivity trends over an extremely wide range of parametric variation. The simple cantilevered (planar) beam example, provided in Figure 3.1 below, demonstrates typical RMA performance ("100%" is baseline). Actual cross-orthogonality checks are also excellent.

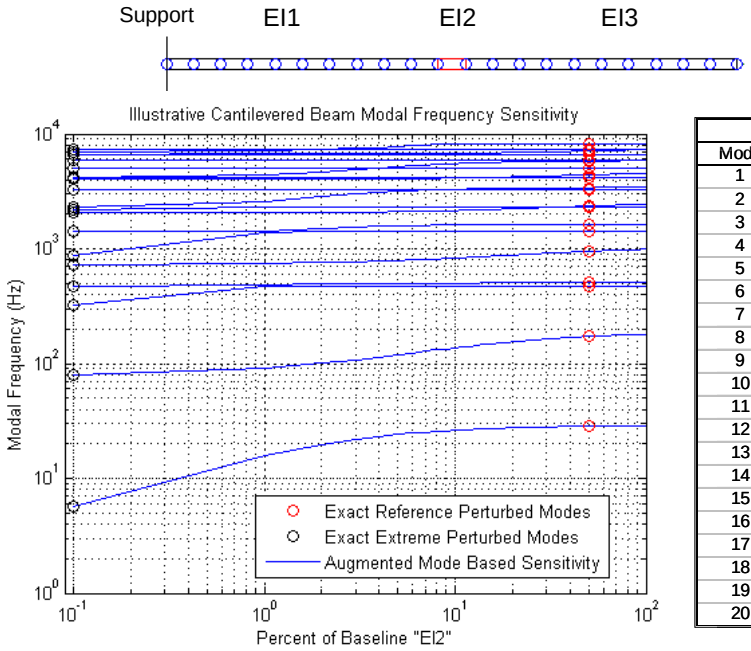

		50% EI2 Loss		99.9% EI2 Loss	
Mode	Baseline	Exact	Approx	Exact	Approx
1	28.78	28.47	28.47	5.71	5.71
2	180.39	172.40	172.40	79.86	79.86
3	467.65	467.65	467.65	320.70	320.70
4	505.11	504.82	504.82	467.65	467.65
5	989.87	950.46	950.46	733.08	733.08
6	1400.30	1400.30	1400.30	870.15	870.15
7	1636.50	1633.60	1633.60	1400.30	1400.30
8	2325.20	2325.20	2325.20	2042.60	2042.60
9	2445.00	2357.10	2357.10	2170.70	2170.70
10	3237.10	3237.10	3237.10	2325.20	2325.20
11	3416.00	3403.70	3403.70	3237.10	3237.10
12	4130.80	4130.80	4130.80	4017.60	4017.60
13	4550.00	4403.90	4403.90	4130.80	4130.80
14	5001.50	5001.50	5001.50	4201.20	4201.20
15	5844.20	5813.10	5813.10	5001.50	5001.50
16	5848.10	5844.20	5844.20	5844.20	5844.20
17	6654.20	6654.20	6654.20	6654.20	6654.20
18	7311.70	7104.70	7104.70	6668.30	6668.30
19	7427.00	7427.00	7427.00	6935.70	6935.70
20	8158.30	8158.30	8158.30	7427.00	7427.00

Figure 3.1. RMA Sensitivity Performance for a Cantilevered Beam Example

3.4 ISPE Convergence Study

During the past year, an early finite element model of the ISPE test article, provided by Dr. Eric Stewart of NASA/MSFC, was employed for an RMA convergence study (see Appendix C). Details of the ISPE model with parametric sensitivity regions are summarized below in Figure 3.2.

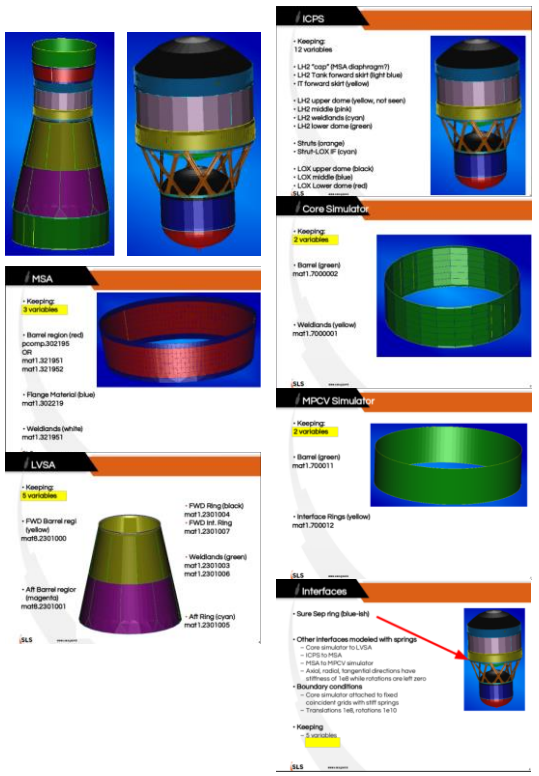

Element	Subcomponent Perturbed	Run #
Nominal Run	---	1
MSA	Barrel Region	2
	Flange Material	3
	Weldlands	4
LVSA	Aft Barrel Region	5
	FWD Barrel Region	6
	Weldlands	7
	FWD Ring	8
	Aft Ring	9
ICPS	LOX Tank Lower dome	10
	LOX Tank Middle	11
	LOX Tank Upper Dome	12
	LH2 Tank Lower dome	13
	LH2 Tank Middle	14
	LH2 Tank Middle Welds	15
	LH2 Tank Upper Dome	16
	Struts	17
	Strut-LOX IF	18
	LH2 tank Forward Skirt	19
	Intertank Forward Skirt	20
Sure Sep	Sure Sep	21
Core Simulator	Barrel	22
	Weldlands	23
MPCV Simulator	Barrel	24
	Interface Rings	25
Integration	MPCV Sim to MSA	26
	Core Sim to LVSA	27
	MSA to ICPS	28
	Core Sim to Ground	29

Negligible Sensitivity

Figure 3.2. ISPE Finite Element Model and Parametric Sensitivity Regions

In response to very significant concerns brought up by Dr. Eric Stewart regarding RMA solution convergence, an investigation of the matter was conducted. Specifically, the role of the SVD tolerance parameter (tol), defined in equation 26, was evaluated. An objective convergence criterion was developed based on comparison of parametric alterations resulting from the solution of the exact modal equation,

$$\left[K_O + \sum_i p_i \Delta K_i\right]\left[\Phi_e\right] = \left[M_O + \sum_i p_i \Delta M_i\right]\left[\Phi_e\right]\left[\lambda_e\right], \tag{31}$$

and the approximate modal equations (see equations 28-30, developed for a specific value of "tol"),

$$\left[k_O + \sum_i p_i \Delta k_i\right]\left[\varphi_a\right] = \left[m_O + \sum_i p_i \Delta m_i\right]\left[\varphi_a\right]\left[\lambda_a\right]$$
$$\left[\Phi\right] = \left[\overline{\Phi}_{OL}\right]\left[\varphi\right]. \tag{32}$$

The metric for evaluation of approximate solution convergence is the cross-orthogonality matrix associated with exact and approximate (RMA) modal sets; specifically

$$\left[COR_{ea}\right] = \left[\Phi_e^T\right]\left[M_O\right]\left[\Phi_a\right] \tag{33}$$

Convergence of the approximate (RMA) modal set is therefore judged on the basis of how close the (absolute value) cross-orthogonality matrix is to an identity matrix. In addition, the difference between exact and approximate corresponding modal frequencies is also employed as part of convergence evaluation.

Before engaging in the actual RMA convergence study, a preliminary evaluation of modal sensitivities for each of the 28 parametric variations (parameter change set to a value of p_i=1) was conducted, wherein the cross-orthogonality between the baseline modes and exact perturbed modes,

$$[\mathrm{COR}_{eO}] = [\Phi_e^T][\mathrm{M}_O][\Phi_O], \tag{34}$$

and corresponding modal frequencies were evaluated. Results of that exercise, summarized below in Table 3.1, indicate that 13 of the total of 28 parametric variations were insignificant.

Table 3.1. Evaluation of the Significance of ISPE Model Parametric Variations

Case	DF (%)	100-Cor (%)	Class
1.2c.mat	4	31	Sensitive
1.3c.mat	5	30	
1.4c.mat	9	17	
1.5c.mat	13	97	
1.6c.mat	13	90	
1.7c.mat	2	35	
1.8c.mat	1	3	Insensitivr
1.9c.mat	1	7	
1.10c.mat	0	0	
1.11c.mat	1	7	
1.12c.mat	1	10	
1.13c.mat	2	81	Sensitive
1.14c.mat	4	22	
1.15c.mat	0	0	Insensitive
1.16c.mat	0	1	
1.17c.mat	2	8	
1.18c.mat	23	95	Sensitive
1.19c.mat	1	6	Insensitive
1.20c.mat	6	93	Sensitive
1.21c.mat	3	89	
1.22c.mat	2	15	
1.23c.mat	23	100	
1.24c.mat	16	100	
1.25c.mat	8	2	
1.26c.mat	28	100	
1.27c.mat	0	0	Insensitive
1.28c.mat	0	0	
1.29c.mat	0	0	
1.30c.mat	0	0	

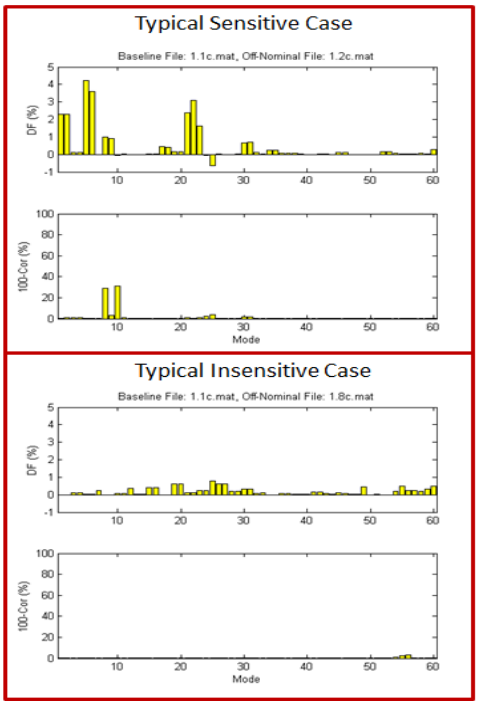

It should be noted that the numerical values provided in the above table are the peak frequency and cross-orthogonality alterations associated with the lowest 60 normal modes of each "unit" parametric variation. As a result of this finding, only the "sensitive" 16 parameters were evaluated in the RMA convergence study.

Results associated with the RMA convergence study, which used "unit" parametric variations and values of "tol" set to 1e-4, 1e-5, and 1e-6, respectively, are summarized below in Table 3.2.

Table 3.2. Summary of RMA Convergence Study Results

Tolerance	1.00E-04		1.00E-05		1.00E-06	
Residuals	65		160		291	
Case	|Δf| (%)	|ΔC| (%)	|Δf| (%)	|ΔC| (%)	|Δf| (%)	|ΔC| (%)
1.2c.mat	1.5	11	1.2	10	0.1	3
1.3c.mat	2.3	16	1.9	16	0.0	1
1.4c.mat	3.2	33	1.6	29	0.1	1
1.5c.mat	1.0	16	0.5	1	0.2	0
1.6c.mat	1.3	1	1.0	3	0.1	0
1.7c.mat	0.4	8	0.4	4	0.1	0
1.13c.mat	0.3	12	0.1	2	0.0	0
1.14c.mat	2.5	16	0.6	5	0.0	0
1.18c.mat	0.7	19	0.1	0	0.0	0
1.20c.mat	3.0	20	1.4	7	0.1	2
1.21c.mat	0.7	15	0.3	1	0.0	1
1.22c.mat	0.4	7	0.2	1	0.1	1
1.23c.mat	1.0	4	0.5	3	0.1	0
1.24c.mat	0.1	0	0.1	0	0.0	0
1.25c.mat	1.7	99	0.6	6	0.1	1
1.26c.mat	0.9	5	0.2	2	0.0	0

Notes for Table 3.2:

(1) |Δf| (%) = [approximate – exact frequency]/[exact frequency] (%)

(2) |ΔC| (%) = 100% - [Cross-Orthogonality] (%)

(3) Values of |Δf| and |ΔC| are the envelopes associated with the lowest 60 system modes

(4) Further details are provided in Appendix C.

It is clear from the above results that tol = 1e-6 produces highly converged RMA modes for the ISPE.

3.5 Conclusions

Alteration of a structural dynamic model for the purpose of reconciliation with respect to measured data typically requires moderate to large variation in (stiffness and/or mass) parameters. Moreover, even when small parametric variations of parameters are required, close spacing of system modes produces large variations in modal vectors. Therefore, modal derivatives are not well suited for tracking of parametric sensitivities of structural dynamic modes. A more robust strategy for approximate modal sensitivity analysis employs the Ritz method. Specifically, a strategy known as Structural Dynamic Modification (SDM) employs a truncated set of baseline system modes as trial vectors to define reduced order mass and stiffness matrices. SDM is a mathematically stable method for approximate parametric sensitivity analysis; however, the baseline system modes are often not adequate for accurate tracking of sensitivities.

Residual Mode Augmentation (RMA) is a methodology that defines trial vectors that augment baseline structure modes, resulting in substantially improved the ability of SDM to efficiently track parametric sensitivities of structural modes. RMA employs (a) system modes associated with large reference parametric alterations and (b) Singular Value Decomposition (SVD) to define a reduced set of residual vectors that are rich in dominant geometric changes experienced by the subject structural system. Since its introduction in 2001, RMA has been successfully employed during several modal tests and a variety of mathematical model studies. Most recently, RMA was employed to investigate parametric sensitivities for

the ISPE structure. As a result of this work, two enhancements of the method have been introduced, namely:

1. Preliminary screening of candidate parametric sensitivities based on reference frequency shifts and cross-orthogonality metrics was defined to differentiate “sensitive” from “insensitive” cases (eliminating “insensitive” parametric variations from further consideration).
2. A frequency and cross-orthogonality (SVD) convergence metric for determination of an augmented residual trial vector set that satisfies RMA accuracy requirements.

3.6 References

[1] “International Space Station P5 Modal Survey: Test Planning through FEM Reconciliation”, R. Coppolino, IMAC 20, 2002

[2] “Rates of Change of Eigenvalues and Eigenvectors”, R. I. Fox and M. P. Kapoor, AIAA Journal, Vol. 6, 1968

[3] “Simplified Calculation of Eigenvector Derivatives”, R. B. Nelson, AIAA Journal, Vol 14, 1976,

[4] "Über eine neue Methode zur Lösung gewisser Variationsprobleme der mathematischen Physik”, W. Ritz, J. reine angew. Math. 135, 1908.

[5] “Twenty Years of Structural Dynamic Modification-A Review, IMAC 20, 2002

[6] “A Hybrid Method for Component Mode Synthesis”, R. MacNeal, Computers and Structures, Vol. 1, 1971

[7] “Structural Mode Sensitivity to Local Modification”, R. Coppolino, SAE Paper 811044, 1981

4.0 Part 2: Mode Consolidation

4.1 Introduction

Natural frequencies and mode shapes of thin shell construction launch vehicle assemblies (and other structures, notably offshore jacket platforms) are ideally grouped in (a) body mode families (e.g. bending, axial, torsion and "bulge" [especially fluid-filled tanks]) and (b) breathing mode families. Breathing modes tend to occur well within the frequency band of fundamental body modes. In addition, breathing modes (especially those associated with singly curved, cylindrical regions) are strongly sensitive to static internal pressure and "weight" structural loading. In contrast, body modes tend to be insensitive to static loadings (as a general rule). Structural features and imperfections (especially in joints) tend to produce structural modes of thin shell structures with mixed body and breathing characteristics, which are sometimes referred to as "weakly coupled" or "fragmented" modes[1]. The mixed character modes often appear as repeated body modes, differing from one another merely due to the magnitude and phase of breathing kinetic energy contributions.

Consolidation of mixed body-breathing modes of a detailed thin shell structure finite element model is easily accomplished by application of either the Harmonic Reduction (HR)[2] or Modified Guyan Reduction (MGR)[3] method, which directly estimates approximate body dominant modes, while suppressing shell breathing modal characteristics. However, corresponding experimental modes of mixed body-breathing character are difficult to categorize and discern.

Due to the likelihood that measured thin shell structure modes will be of mixed body-breathing character, (1) a modal test requires thorough instrumentation and exciter resources to clearly map the subject system's modes and (2) a sufficiently detailed finite element model that describes all anticipated body and breathing modes in the frequency band of interest. Employment of a systematic modal test planning procedure (e.g., RKE[4] and IRKE[5]) defines an instrumentation array that will properly map all modes in the frequency band of interest.

This paper introduces a procedure for consolidation of mixed character (body-shell breathing) experimental modes that processes modal kinetic energy clusters via singular value decomposition. The estimated consolidated body natural frequencies and mode shapes are found to be in close agreement with both HR and MGR consolidated body modes of an illustrative example shell structure.

4.2 Nomenclature

Symbol	Definition
F	force
K	stiffness
KE	kinetic energy
M	mass
OR	orthogonality
U	displacement
f	frequency
m	generalized mass
p	sensitivity parameter
q	modal displacement
u	generalized displacement
Γ	force allocation array
I	identity matrix
Φ	mode shape
Ψ	displacement allocation array
γ	modal cluster SVD eigenvalue
λ	eigenvalue
υ	modal cluster SVD eigenvector
φ	generalized mode shape

Subscript	Definition
$[\,]_L$	lower frequency modes
$[\,]_b$	body modes
$[\,]_r$	remaining, breathing modes
$[\,]_n$	modal
$[\,]_c$	consolidated modes

Acronym	Definition
CGR	Classical Guyan Reduction
DOF	Degree of Freedom
HR	Harmonic Reduction
MGR	Modified Guyan Reduction
TAM	Test Analysis Model

4.3 Model Order Reduction Techniques and System Mode Classification Metrics

Classical Guyan Reduction (CGR)[6] has been a mainstay in the aerospace community since its introduction in 1965. CGR was originally intended to permit modal analysis of "large" finite element models that were beyond the practical solution capabilities of most computers. Since that time, computers and numerical methods have achieved the capability to treat extremely large, sparse real and complex eigenvalue problems. The primary reason for continued employment of CGR today is for definition of the Test-Analysis Model (TAM) mass matrix that corresponds to the planned measured response array for modal testing[4,5].

4.3.1 Harmonic Reduction (HR)

A noteworthy alternative to CGR is a technique termed "Harmonic Reduction" or HR[2], which was an attempt to efficiently and effectively reduce large-order NASTRAN hydroelastic propellant tank models. In that endeavor, discrete DOFs were replaced with harmonic "patches" that defined displacement transformations of the type,

$$\{U\} = \begin{bmatrix} \Psi_{11} & 0 & \dots & 0 \\ 0 & \Psi_{22} & \dots & 0 \\ \dots & \dots & \dots & \dots \\ 0 & 0 & \dots & \Psi_{kk} \end{bmatrix} \begin{Bmatrix} U_1 \\ U_2 \\ \dots \\ U_k \end{Bmatrix} = [\Psi_{HR}]\{u\} \tag{1}$$

Employing $[\Psi_{HR}]$ as Ritz vectors, the reduced HR stiffness and mass matrices are

$$[K_{HR}] = [\Psi_{HR}]^T [K][\Psi_{HR}], \quad [M_{HR}] = [\Psi_{HR}]^T [M][\Psi_{HR}]. \tag{2}$$

4.3.2 Modified Guyan Reduction (MGR)

Modified Guyan Reduction (MGR)[3] is the direct result of a conversation with Dr. Paul Blelloch of ATA, who informed the writer of difficulties encountered with Classical Guyan Reduction (CGR) during test planning for a complex structure modeled, in-part, with 3-D elastic solid elements. Recalling that CGR is based on static deflection patterns associated with point loads, coupled with the fact that 3-D elastic

deflections under concentrated loadings are infinite, a distributed "patch" load approach (MGR) was defined to circumvent the CGR difficulty. Since 2011, the new, MGR method has been applied to other challenging situations and continuing evaluations have produced related developments.

Consider the general distribution of static loads described by the matrix equation,

$$\{F\} = \begin{bmatrix} \Gamma_{11} & 0 & \dots & 0 \\ 0 & \Gamma_{22} & \dots & 0 \\ \dots & \dots & \dots & \dots \\ 0 & 0 & \dots & \Gamma_{kk} \end{bmatrix} \begin{Bmatrix} F_1 \\ F_2 \\ \dots \\ F_k \end{Bmatrix} = [\Gamma]\{F_\Gamma\}, \tag{3}$$

where the individual load patches, $[\Gamma_{ii}]$, represents unit load patterns (over each specific geometric patch) that are mathematically the transposes of rigid body deflection patterns. The static displacement due to the above defined loading is

$$\{U\} = [K]^{-1}\{F\} = [K^{-1}\Gamma]\{F_\Gamma\}. \tag{4}$$

Pre-multiplication of this result by the transpose of unit loadings yields,

$$\{U_\Gamma\} = [\Gamma]^T[K]^{-1}\{F\} = [\Gamma^T K^{-1}\Gamma]\{F_\Gamma\}, \quad \{F_\Gamma\} = [\Gamma^T K^{-1}\Gamma]^{-1}\{U_\Gamma\}. \tag{5}$$

Substitution of this result into equation 4 yields the (load patch based) MGR transformation,

$$\{U\} = [K^{-1}\Gamma][\Gamma^T K^{-1}\Gamma]^{-1}\{U_\Gamma\} = [\Psi_{MGR}]\{U_\Gamma\}. \tag{6}$$

Employing $[\Psi_{MGR}]$ as Ritz vectors, the MGR stiffness and mass matrices are

$$[K_{MGR}] = [\Psi_{MGR}]^T[K][\Psi_{MGR}], \quad [M_{MGR}] = [\Psi_{MGR}]^T[M][\Psi_{MGR}]. \tag{7}$$

It should be noted that, in the limiting case of concentrated, point patch loads, the present formulation reduces to CGR.

4.3.3 Approximate Modes of the Reduced Order System

Regardless of the selected model reduction strategy (CGR, HR, MGR), the original system is using the generic reduction transformation,

$$\{U\} = [\Psi]\{u\} \tag{8}$$

Resulting in the generic reduced order mass and stiffness matrices,

$$[K_{\Psi\Psi}] = [\Psi]^T[K][\Psi], \quad [M_{\Psi\Psi}] = [\Psi]^T[M][\Psi]. \tag{9}$$

The modal transformation resulting from analysis of the reduced-order system is therefore,

$$\{u\} = [\varphi]\{q\}, \tag{10}$$

with corresponding approximate natural frequencies (for orthonormal modal vectors),

$$(2\pi f_n)^2 = \{\varphi_n\}^T[K_{\Psi\Psi}]\{\varphi_n\} \tag{11}$$

Approximate mode shapes, expressed in terms of the original unreduced DOF set are

$$[\Phi_\Psi] = [\Psi][\varphi] \tag{12}$$

4.3.4 Body and Breathing Modes of Axisymmetric Shell Structures

The shell structure, shown below in Figure 4.1, serves as an illustrative example system for the present discussion (further details are found in Appendix D). It consists of five substructures, namely (1) a lower cylindrical skirt (fully fixed at its base), (2) a lower hemispherical bulkhead, (3) lower cylindrical section, (4) upper cylindrical section, and (5) upper hemispherical bulkhead. The overall dimensions of the aluminum structure are length, L=100 inches, radius, R=20 inches, and wall thickness, h=0.4 inches. It should be noted that this illustrative example structure does not represent a realistic design. The rather high thickness-to-radius ratio, h/R=1/50, was selected to produce less shell breathing modes in the base frequency band (f < 2000 Hz) than typical aerospace systems, while including modes of sufficient complexity to illustrate key aspects of quantitative normal mode metrics.

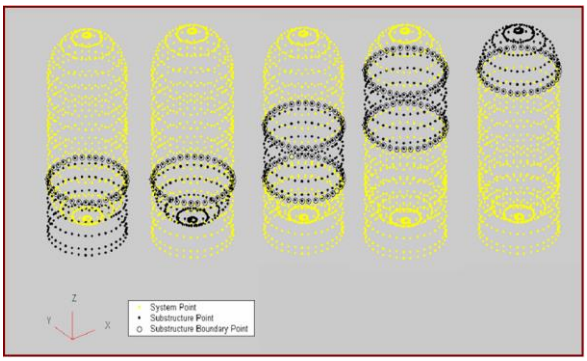

Figure 4.1. Illustrative Example Axisymmetric Shell Structure

There are a variety of metrics for characterization of normal modes, namely (a) modal effective mass (for a supported structure), (b) directional kinetic energy distribution, (c) component kinetic and strain energy distribution (when the structure is appropriately segmented into separate individual components), and (d) kinetic energy distribution in terms of "body" and "breathing" modes. While all of the above characterization metrics are discussed in references 7 and 8, the present discussion focuses on the fourth category.

Consider the following (Figure 4.2) seven "body" geometric patterns for the example shell axial stations (which may be used for either HR or MGR purposes).

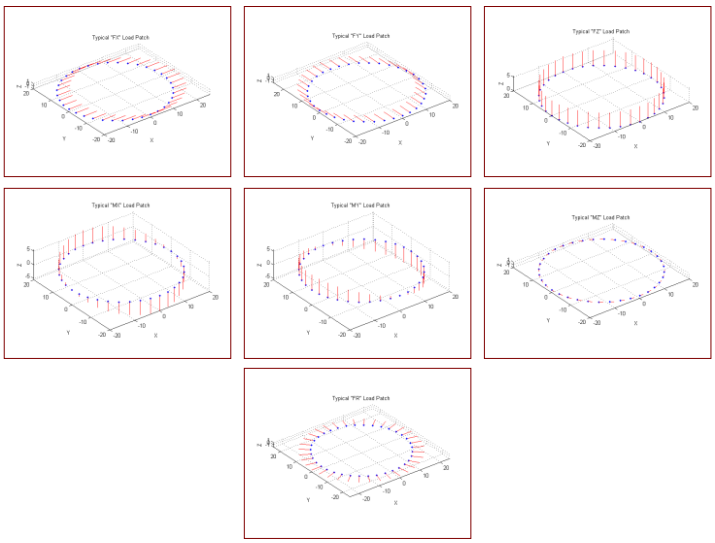

Figure 4.2. Shell Axial Station "Body" Geometric Patterns

The seven patterns are associated with cross-sectional lateral ("TX" and "TY"), and axial ("TZ") translations, pitch, yaw and torsional ("RX","RY", and "RZ") rotations, and radial bulge ("TR") translation. In "circumferential harmonic terms, the above seven patterns represent N=0 and 1 motions (or load patterns).

By organizing the above described geometric patterns as a body displacement transformation matrix, $[\Psi_b]$, the discrete lower frequency FEM shell displacements, $[\Phi_L]$, are expressed as,

$$[\Phi_L] = [\Psi_b][\varphi_b] + [\Phi_r] \tag{13}$$

where $[\Psi_b]$ may be either defined as $[\Psi_{HR}]$ or $[\Psi_{MGR}]$. In actuality, $[\Psi_{HR}]$ has been selected for the present discussion and illustrative example analysis.

Employing linear least-squares analysis, as follows, each system normal mode may be partitioned into "body" and (remainder) "breathing" components.

$$[\Psi_b^T M \Phi_L] = [\Psi_b^T M \Psi_b][\varphi_b] + [\Psi_b^T M \Phi_r] = [\Psi_b^T M \Psi_b][\varphi_b] + [0] \rightarrow [\varphi_b] = [\Psi_b^T M \Psi_b]^{-1}[\Psi_b^T M \Phi_L] \tag{14}$$

$$[\Phi_b] = [\Psi_b][\varphi_b],\ [\Phi_r] = [\Phi_L] - [\Phi_b],\ [\Phi_b^T M \Phi_r] = [0] \text{ (orthogonality of body and breathing)}$$

Due to orthogonality of the body and breathing modal displacement components, the following kinetic energy metrics are defined:

$$[I_L] = [\Phi_L^T M \Phi_L] = [\Phi_b^T M \Phi_b] + [\Phi_r^T M \Phi_r] \text{ (Total modal KE = total body KE + total breathing KE)} \tag{15}$$

$$[M\Phi_L] \otimes [\Phi_L] = [M\Phi_b] \otimes [\Phi_b] + [M\Phi_r] \otimes [\Phi_r] \text{ (Body and breathing KE distributions)}$$

The total modal kinetic energy and partial kinetic energies for each individual mode are the diagonal terms of the first matrix equation set of "equation" 10. A summary of ideal axisymmetric shell structure modal frequencies and kinetic energy metrics is presented below in Figure 4.3.

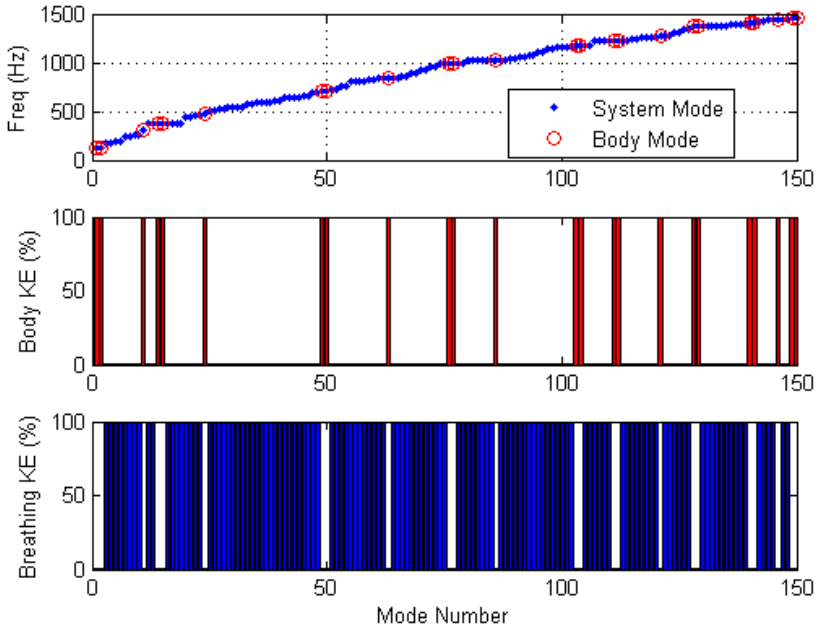

Figure 4.3. Axisymmetric Shell Structure Modal Frequencies and Kinetic Energy Metrics

4.3.5 MGR and HR Approximations for the Perfectly Axisymmetric Shell Structure

HR and MGR strategies produce approximate modal solutions for body dominant modes, which are summarized below in Table 4.1, along with exact body dominant modes for the ideal axisymmetric shell structure. The MGR modal kinetic energy distributions, based on partial generalized displacement (TX, TY, TZ, RX, RY, RZ, and TR) sums clearly indicate the nature of each body dominant mode.

Table 4.1. Comparison of Exact, HR and MGR Body Modes

Exact			Harmonic Reduction		MGR		MGR KE Distribution						
Mode	Freq (Hz)	Type	Mode	Freq (Hz)	Mode	Freq (Hz)	TX	TY	TZ	RX	RY	RZ	TR
1	122.20	Bend-Y	1	122.20	1	122.20		96		4			
2	122.20	Bend-X	2	122.20	2	122.20	96				4		
11	315.24	Torsion	3	315.24	3	315.24						100	
14	377.21	Bend-Y	4	377.21	4	377.23		91		9			
15	377.21	Bend-X	5	377.21	5	377.24	91				9		
24	467.77	Axial	6	467.78	6	467.78			100				
49	706.65	Bend-Y	7	706.84	7	706.86		91		9			
50	706.65	Bend-X	8	706.85	8	706.87	91				9		
63	841.31	Torsion	9	841.35	9	841.35						100	
76	997.48	Lateral-Y	10	999.12	10	997.81		60		40			
77	997.50	Lateral-X	11	999.14	11	997.83	60				40		
86	1029.90	Axial	12	1031.30	12	1030.10			94				6
103	1169.60	Lateral-Y	13	1174.20	13	1170.00		60		40			
104	1169.60	Lateral-X	14	1174.30	14	1170.10	60				40		
111	1223.50	Bend-Y	15	1233.80	15	1224.10		91		9			
112	1223.50	Bend-X	16	1233.80	16	1224.10	91				9		
121	1273.40	Axial-Bulge	17	1281.00	17	1273.60			78				22
128	1368.30	Bend-Y	18	1395.10	18	1369.10		95		5			
129	1368.40	Bend-X	19	1395.10	19	1369.20	95				5		
140	1402.80	Lateral-XY	20	1416.30	20	1404.50	7	8		45	40		
141	1402.80	Lateral-XY	21	1416.30	21	1404.50	8	8		40	44		
146	1440.40	Bulge-Axial	22	1466.60	22	1440.40			45				55
149	1452.70	Lateral-XY	23	1467.50	23	1453.60	33	43		14	11		
150	1452.70	Lateral-XY	24	1484.70	24	1453.60	43	33		11	14		

The above results indicate that MGR based natural frequencies follow exact structure body dominant modal frequencies more accurately than the HR based approximation.

4.3.6 Body and Breathing Modes of a Perturbed Axisymmetric Shell Structure

As a general rule, as-built geometrically axisymmetric shell structures are not structurally axisymmetric due to local design features and imperfections. The effects of typical perturbations are evaluated herein by addition of a "X=0" axial line of added mass (total value is 1.85% of the baseline shell rigid body mass) on the example shell (previously illustrated in Figure 4.1). A summary of perturbed axisymmetric shell structure modal frequencies and kinetic energy metrics is presented below in Figure 4.4.

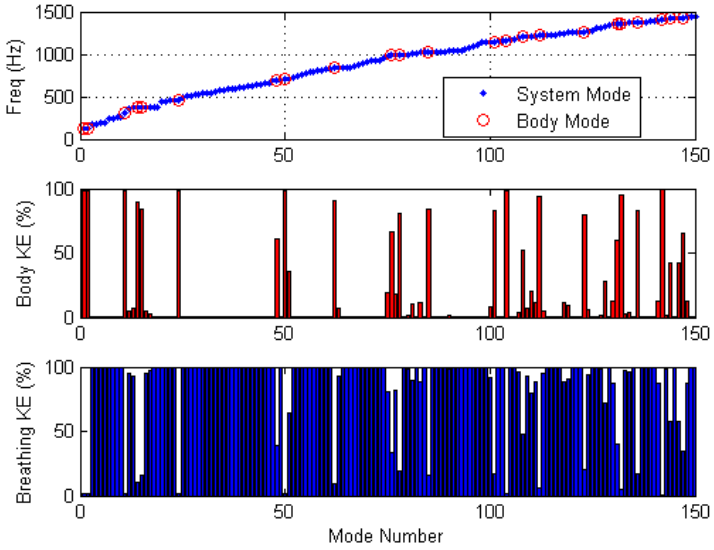

Figure 4.4. Perturbed Shell Structure Modal Frequencies and Kinetic Energy Metrics

Applying the body-breathing metrics (equations 8-10) to the perturbed shell structure to categorize modes that are body kinetic energy dominant, forty-nine (49) modes of the perturbed system are found to have "body" kinetic energy in excess of 2%. The 49 perturbed system modes are now compared to the 24 pure "body" modes of the ideal axisymmetric structure employing the cross-orthogonality matrix (using the axisymmetric structure mass matrix as a reference). Results showing absolute values of cross-orthogonality in excess of 5% are provided in below in Table 4.2.

Table 4.2. Cross-Orthogonality of Ideal Axisymmetric & Perturbed Shell Body Dominant Modes

			Ideal Axisymmetric Shell																						
	Mode		1	2	11	14	15	24	49	50	63	76	77	86	103	104	111	112	121	128	129	140	141	146	149
		Freq (Hz)	122.20	122.20	315.24	377.21	377.21	467.77	706.65	706.65	841.31	997.48	997.50	1029.9	1169.6	1169.6	1223.5	1223.5	1273.4	1368.3	1368.4	1402.8	1402.8	1440.4	1452.7
Perturbed Axisymmetric Shell	1	120.97	99																						
	2	121.13		99																					
	11	312.43			99																				
	12	359.94				24																			
	13	367.98				27																			
	14	373.97					95																		
	15	374.65				92																			
	16	375.36					23																		
	17	377.43					16																		
	24	463.45						99																	
	48	695.39							78																
	50	701.56								99															
	51	706.21							60																
	62	833.52									95														
	63	836.13									26														
	75	967.62										44													
	76	986.08										82		7											
	77	992.77											43												
	78	994.38											90												
	81	1001.8										31													
	83	1017.4												34											
	85	1020.4										6		91											
	100	1148.6													29										
	101	1149.7													91		5								
	104	1166.4														99									
	107	1187.2													9		15		7						6
	108	1200.1													7		71								
	109	1205.5													12		22								
	110	1210.2													8		43		10						
	111	1212.5															33		7						
	112	1219.5																97							
	113	1221.3																23							
	118	1237.1																	32						
	119	1252.5															21		22						
	123	1266.5															5		89						
	124	1275.8													8		20			10					
	128	1322.5															6			51					
	130	1352.8																		33		9		8	
	131	1363.1																		65		41		7	
	132	1366.3																			98				
	133	1366.4																		5		12		3	
	134	1368.8																			21				
	136	1373.7																		36		83		9	
	141	1395.2																				15		24	
	142	1402.0																					100		
	144	1419.6																						23	58
	146	1422.6																						38	52
	147	1433.2																				10		79	
	148	1434.8																						18	31

Introduction of a perturbation to the ideal axisymmetric shell structure has the effect of "fragmenting" or "splitting" the ideal axisymmetric system's body-dominant modes. The naming and characterization of experimental body-dominant modes is no longer a straightforward process. Moreover, estimation of specific experimental "body" mode frequencies is problematic.

4.3.7 Additional Modal Sensitivity Trends for the Perturbed Shell Structure

Additional insight into modal sensitivity for the example shell structure is gained by variation of the magnitude of added line mass from 0 to 3.7% (the sensitivity parameter, p, varies from 0 to 2). Sensitivity of all system modes in the 0-1400 Hz frequency band, along with tagged modal subsets with body kinetic energy $\geq 25\%$, $\geq 50\%$, and $\geq 75\%$ respectively, is illustrated below in Figure 4.5.

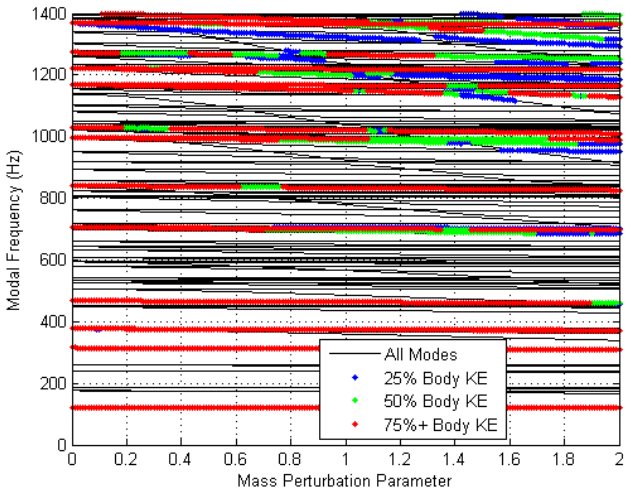

Figure 4.5. Sensitivity of Perturbed Shell System Modes to Added Line Mass

The above results indicate that body dominant (body KE ≥ 75%) modal frequencies are generally insensitive to added line mass (0-3.7% of total system mass), while some breathing mode frequencies (especially body KE ≤ 25%) exhibit much greater frequency sensitivity.

4.4 Body Mode Consolidation

While there appears to be a series of options for understanding and categorization of structural modes for shell-type structures (as well as other built-up systems), "fragmentation" or "splitting" of body dominant modes represents a challenge that cannot necessarily be easily circumvented when modal data is experimental (as noted in ISPE experimental modal data). Moreover, since SLS component and system finite element models are highly detailed, the same challenges occur when non-reduced normal modes and modal sensitivities are computed.

4.4.1 Modal Cluster Definition Using the Perturbed Shell Model Example

Recalling the previous discussion in Section 3.4, the body displacement transformation matrix, $[\Phi_b]$, is used to decompose the discrete lower frequency FEM shell modal displacements, $[\Phi_L]$, into "body" and remaining ("breathing") components, respectively,

$$[\Phi_L] = [\Phi_b] + [\Phi_r], \text{ where } [\Phi_b] = [\Psi_b][\varphi_b]. \tag{16}$$

Since the "body" and "breathing" modal components are mutually orthogonal (see equations 8-10), the modal orthogonality matrix (which is also the modal kinetic energy matrix) is the sum of two components, namely,

$$[OR] = [m_b] + [m_r] = [I], \text{ where } [m_b] = [\Phi_b^T M \Phi_b], \ [m_r] = [\Phi_r^T M \Phi_r]. \tag{17}$$

The process of mode consolidation focuses on mathematical operations on "clusters" within the body mode orthogonality matrix, $[m_b]$, and the associated lower eigenvalues of the complete structural system, $[\lambda_L]$.

The body mode orthogonality matrix, $[m_b]$, for the perturbed example shell structure (p=1) from the previous section is depicted below in Figure 4.6 as a Matlab "pseudocolor" graphic of absolute values for $[m_b]$.

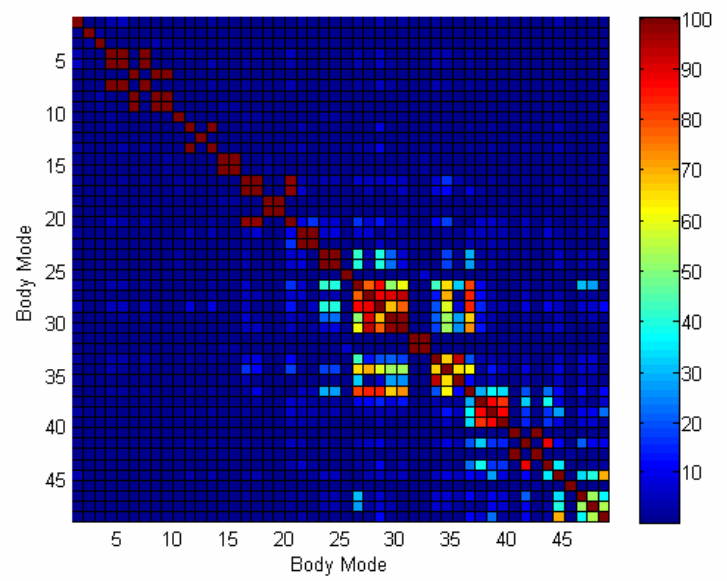

Figure 4.6. Body Mode Orthogonality Matrix, $[m_b]$, Absolute Values

It should be noted that the body modes were normalized to unit modal mass to generate a version of $[m_b]$ with unit diagonal terms, thus accentuating the repeated nature of clustered modes. Apparently repeated and highly coupled body mode clusters are readily "tagged" among the 49 body modes (selected based on individual body mode kinetic energy, $[m_b]_{ii} \geq 10\%$, body modes that have not been not renormalized).

The following rule is employed to define body mode clusters, with their selection depicted in Figure 4.7:

$$\left|m_b\right|_{ii} \geq 0.10 \,,\ \left|m_b\right|_{ij} \geq 0.10 \ \text{ for } i \neq j \tag{18}$$

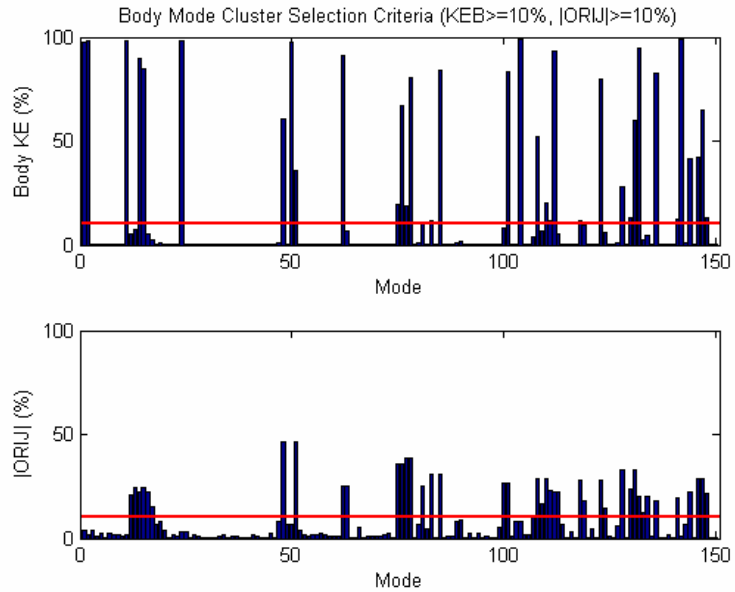

Figure 4.7. Body Mode Cluster Selection Criterion (note KEB = $|m_b|_{ii}$, |ORIJ| = $|m_b|_{ij}$)

Eight body mode clusters are defined using the above defined criteria. They are depicted below for body dominant modes 1-22 and 23-49, respectively in Tables 4.3 and 4.4.

Table 4.3. Mode Clusters for Body Dominant Modes 1-22

Perturbed (Selected Modes)				Body Mode Orthogonality Matrix																				
Mode	Freq (Hz)	diag (OR)	coup(OR)	1	2	3	4	5	6	7	8	9	10	11	12	13	14	15	16	17	18	19	20	21	22
1	120.97	98	2	98	0	0	1	-2	0	0	0	0	-1	1	0	1	0	0	0	0	0	0	0	-1	0
2	121.13	98	2	0	98	-2	0	0	0	0	0	0	0	0	0	0	0	0	0	0	0	0	0	0	0
11	312.43	98	2	0	-2	98	0	0	-1	0	-1	0	0	0	0	0	0	0	0	0	0	0	0	0	0
12	359.94	5	21	1	0	0	5	6	0	21	0	0	0	0	0	0	0	0	0	0	0	0	0	0	0
13	367.98	7	25	-2	0	0	6	7	0	25	0	0	0	0	0	1	0	0	0	0	0	0	0	0	0
14	373.97	90	22	0	0	-1	0	0	90	0	-22	-15	0	0	0	0	1	0	0	0	0	0	0	0	0
15	374.65	84	25	0	0	0	21	25	0	84	0	0	0	1	0	1	0	0	-1	0	0	0	-1	0	0
16	375.36	5	22	0	0	-1	0	0	-22	0	5	4	0	0	0	0	0	0	0	0	0	0	0	0	0
17	377.43	3	15	0	0	0	0	0	-15	0	4	3	0	0	0	0	0	0	0	0	0	0	0	0	0
24	463.45	98	2	-1	0	0	0	0	0	0	0	0	98	0	0	0	0	0	-1	-1	0	0	0	0	0
48	695.39	61	46	1	0	0	0	0	0	1	0	0	0	61	0	-46	0	0	-1	0	0	0	0	-1	0
50	701.56	98	0	0	0	0	0	0	0	0	0	0	0	0	98	0	0	0	0	0	0	0	0	0	0
51	706.21	36	46	1	0	0	0	1	0	1	0	0	0	-46	0	36	0	0	0	0	0	0	0	1	0
62	833.52	91	25	0	0	0	0	0	1	0	0	0	0	0	0	0	91	25	0	0	1	0	0	0	0
63	836.13	7	25	0	0	0	0	0	0	0	0	0	0	0	0	0	25	7	0	0	0	0	0	0	0
75	967.62	20	36	0	0	0	0	0	0	-1	0	0	-1	-1	0	0	0	0	20	36	0	0	-14	-1	1
76	986.08	67	36	0	0	0	0	0	0	0	0	0	-1	0	0	0	0	0	36	67	0	0	-25	-2	-1
77	992.77	19	39	0	0	0	0	0	0	0	0	0	0	0	0	0	1	0	0	0	19	-39	0	0	0
78	994.38	81	39	0	0	0	0	0	0	0	0	0	0	0	0	0	0	0	0	0	-39	81	0	0	0
81	1001.81	10	25	0	0	0	0	0	0	-1	0	0	0	0	0	0	0	0	-14	-25	0	0	10	-1	-5
83	1017.37	12	31	-1	0	0	0	0	0	0	0	0	0	-1	0	1	0	0	-1	-2	0	0	-1	12	31
85	1020.38	84	31	0	0	0	0	0	0	0	0	0	0	0	0	0	0	0	1	-1	0	0	-5	31	84

Table 4.4. Mode Clusters for Body Dominant Modes 23-49

Perturbed (Selected Modes)				Body Mode Orthogonality Matrix																							
Mode	Freq (Hz)	diag (OR)	coup(OR)	23	24	25	26	27	28	29	30	31	32	33	34	35	36	37	38	39	40	41	42	43	44	45	46	47	48	49
100	1148.56	8	26	8	-26	0	2	1	-3	-3	-1	0	0	0	-2	0	-2	0	0	1	0	0	0	0	1	0	1	-1	0	0
101	1149.73	83	26	-26	83	0	-7	-2	10	9	3	0	0	0	5	-1	6	1	-1	-1	0	0	0	0	-2	0	-2	3	1	1
104	1166.38	99	1	0	0	99	0	0	0	0	0	0	-1	0	0	0	0	0	0	0	0	0	0	0	0	0	0	0	0	0
107	1187.16	4	11	2	-7	0	4	11	-4	4	4	0	0	-3	4	-6	-4	-1	0	0	0	0	0	0	0	0	-4	3	0	-2
108	1200.07	52	29	1	-2	0	11	52	-17	29	23	0	0	-3	15	0	-15	-4	-1	-1	0	1	0	-2	-1	0	-1	1	-1	0
109	1205.54	7	17	-3	10	0	-4	-17	7	-8	-7	0	0	2	-5	2	5	2	0	-1	0	0	0	-2	0	0	1	1	-2	1
110	1210.18	20	29	-3	9	0	4	29	-8	20	15	0	0	3	7	11	-7	-2	-1	0	0	0	0	0	-1	0	1	-1	0	1
111	1212.47	12	23	-1	3	0	4	23	-7	15	12	0	0	2	6	8	-6	-2	0	0	0	0	0	1	-1	0	0	0	0	1
112	1219.50	93	22	0	0	0	0	0	0	0	0	93	22	0	0	0	0	0	0	0	0	0	0	0	0	0	0	0	0	0
113	1221.28	5	22	0	0	-1	0	0	0	0	0	22	5	0	0	0	0	0	0	0	0	0	0	0	0	0	0	0	0	0
118	1237.13	12	28	0	0	0	-3	-3	2	3	2	0	0	12	-7	28	2	1	1	1	0	0	0	0	1	0	1	-2	0	1
119	1252.53	10	18	-2	5	0	4	15	-5	7	6	0	0	-7	10	-18	-5	0	-2	1	0	0	0	-1	-1	0	1	-1	0	2
123	1266.47	80	28	0	-1	0	-6	0	2	11	8	0	0	28	-18	80	2	1	2	0	0	-1	0	-1	2	0	-2	1	-1	-2
124	1275.81	6	15	-2	6	0	-4	-15	5	-7	-6	0	0	2	-5	2	6	-4	3	-6	0	-1	0	5	-1	0	2	0	-2	1
128	1322.55	28	33	0	1	0	-1	-4	2	-2	-2	0	0	1	0	1	-4	28	-17	33	0	3	0	-18	2	0	-1	0	-3	1
130	1352.82	13	24	0	-1	0	0	-1	0	-1	0	0	0	1	-2	2	3	-17	13	-24	0	-1	0	5	3	0	-2	-3	7	-2
131	1363.11	60	33	1	-1	0	0	-1	-1	0	0	0	0	1	1	0	-6	33	-24	60	0	-2	0	11	-2	0	-3	-3	2	-1
132	1366.26	95	20	0	0	0	0	0	0	0	0	0	0	0	0	0	0	0	0	0	95	0	20	0	0	0	0	0	0	0
133	1366.43	2	12	0	0	0	0	1	0	0	0	0	0	0	0	-1	-1	3	-1	-2	0	2	0	-12	1	0	2	-1	-1	1
134	1368.84	4	20	0	0	0	0	0	0	0	0	0	0	0	0	0	0	0	0	0	20	0	4	0	0	0	0	0	0	0
136	1373.70	83	18	0	0	0	0	-2	-2	0	1	0	0	0	-1	-1	5	-18	5	11	0	-12	0	83	-11	0	0	-1	-2	-1
141	1395.25	12	20	1	-2	0	0	-1	0	-1	-1	0	0	1	-1	2	-1	2	3	-2	0	1	0	-11	12	0	-8	-9	20	-5
142	1402.03	99	0	0	0	0	0	0	0	0	0	0	0	0	0	0	0	0	0	0	0	0	0	0	0	99	0	0	0	0
144	1419.64	42	22	1	-2	0	-4	-1	1	1	0	0	0	1	1	-2	2	-1	-2	-3	0	2	0	0	-8	0	42	-22	-19	22
146	1422.59	42	29	-1	3	0	3	1	1	-1	0	0	0	-2	-1	1	0	0	-3	-3	0	-1	0	-1	-9	0	-22	42	-29	-9
147	1433.20	65	29	0	1	0	0	-1	-2	0	0	0	0	0	0	-1	-2	-3	7	2	0	-1	0	-2	20	0	-19	-29	65	-14
148	1434.82	13	22	0	1	0	-2	0	1	1	1	0	0	1	2	-2	1	1	-2	-1	0	1	0	-1	-5	0	22	-9	-14	13

4.4.2 Decomposition of Modal Clusters Using SVD (Mode Consolidation Theory)

Consider an individual modal cluster (see Tables 4.3-4.4) that is defined by the following matrix data:

$[\Phi_b]$ = "body" mode shape cluster (see equation 16)

`$[\lambda]$ = eigenvalues for the system modes from which the cluster is defined

$[m_b]$ = "body" mode cluster generalized mass matrix (see equation 17).

Generalized eigenvectors associated with $[m_b]$ are defined based on the following singular value decomposition operations:

$$[m_b][\tilde{\upsilon}_b] = [\tilde{\upsilon}_b][\gamma_b], \text{ where } [\tilde{\upsilon}_b^T][\tilde{\upsilon}_b] = [I] \text{ and } [\tilde{\upsilon}_b^T][m_b][\tilde{\upsilon}_b] = [\gamma_b], \tag{19}$$

and the calculated eigenvalues are sequenced in descending order ($\gamma_{b,1} \geq \gamma_{b,2} \geq \gamma_{b,3} \geq \ldots$). By employing a cut-off criterion ($\gamma_{b,i} / \gamma_{b,1} \geq$ tol), a truncated subset of eigenvalues and eigenvectors are kept. Finally, the truncated set of cluster eigenvectors is rescaled as,

$$[\upsilon_b] = [\tilde{\upsilon}_b][\gamma_b]^{1/2}, \text{ resulting in } [\upsilon_b^T][\upsilon_b] = [\gamma_b] \text{ and } [m_b] \approx [\upsilon_b][\upsilon_b^T]. \tag{20}$$

The body dominant modal frequencies are finally "consolidated" employing "strain energy" weighted summing employing Rayleigh quotients and associated SVD eigenvectors as,

$$\lambda_{c,i} = \frac{\{\upsilon_{b,i}\}^T [\lambda] \{\upsilon_{b,i}\}}{\{\upsilon_{b,i}\}^T \{\upsilon_{b,i}\}} \rightarrow f_{c,i} = \frac{\sqrt{\lambda_{b,i}}}{2\pi}, \tag{21}$$

where the "c" subscript is used to denote the "consolidated" mode quantity. The corresponding consolidated system mode shapes associated with the consolidated modal frequencies are computed as follows:

$\{\tilde{\Phi}_{c,i}\} = [\Phi_b]\{\upsilon_{b,i}\}$ (Non-normalized, consolidated system mode shape)

$m_{c,i} = \{\tilde{\Phi}_{c,i}\}^T [M] \{\tilde{\Phi}_{c,i}\}$ (Non-normalized modal mass, with respect to the system (TAM) mass matrix) (22)

$\{\Phi_{c,i}\} = \{\tilde{\Phi}_{c,i}\} / m_{c,i}$ (Unit mass normalized, consolidated system mode shape)

The above development is apologetically "heuristic". However, it appears to provide consistent, satisfying results for the example perturbed shell structure (with p=1 and SVD tol=.01), as evidenced in orthogonality of the consolidated body modes shown below in Table 4.5.

Table 4.5. Consolidated Body Mode Set Orthogonality

Mode		1	2	3	4	5	6	7	8	9	10	11	12	13	14	15	16	17	18	19	20	21	22	23
	Freq (Hz)	Orthogonality (%)																						
1	120.97	100	0	0	0	0	-1	0	0	0	0	0	0	0	0	0	0	0	0	0	0	0	0	0
2	121.13	0	100	-2	0	0	0	0	0	0	0	0	0	0	0	0	0	0	0	0	0	0	0	0
3	312.43	0	-2	100	0	1	0	0	0	0	0	0	0	0	0	0	0	0	0	0	0	0	0	0
4	373.36	0	0	0	100	0	1	0	0	0	1	0	0	0	0	0	0	-1	0	0	0	0	0	0
5	374.14	0	0	1	0	100	0	0	0	-1	0	0	0	0	0	0	0	0	0	0	0	0	0	0
6	463.45	-1	0	0	1	0	100	0	0	0	-2	0	0	-2	0	1	0	0	0	0	0	0	0	-1
7	699.42	0	0	0	0	0	0	100	0	0	0	0	1	0	0	0	0	0	0	1	0	0	1	0
8	701.56	0	0	0	0	0	0	0	100	0	0	0	0	0	0	0	0	0	0	0	0	0	0	0
9	833.71	0	0	0	0	-1	0	0	0	100	0	-1	0	0	0	0	0	0	0	0	0	0	0	0
10	983.97	0	0	0	1	0	-2	0	0	0	100	0	-1	-1	0	0	0	-1	0	0	0	0	0	0
11	994.07	0	0	0	0	0	0	0	0	-1	0	100	0	0	0	0	0	0	0	0	0	0	0	0
12	1020.02	0	0	0	0	0	0	1	0	0	-1	0	100	1	0	1	0	0	0	3	0	0	-1	0
13	1149.62	0	0	0	0	0	-2	0	0	0	-1	0	1	100	0	0	0	-1	-1	0	0	0	0	-4
14	1166.38	0	0	0	0	0	0	0	0	0	0	0	0	0	100	0	0	0	0	0	0	0	0	0
15	1210.08	0	0	0	0	0	1	0	0	0	0	0	1	0	0	100	0	0	0	0	0	0	0	1
16	1219.59	0	0	0	0	0	0	0	0	0	0	0	0	0	0	0	100	0	0	0	0	0	0	0
17	1260.33	0	0	0	-1	0	0	0	0	0	-1	0	0	-1	0	0	0	100	0	0	0	0	0	2
18	1359.92	0	0	0	0	0	0	0	0	0	0	0	0	-1	0	0	0	0	100	0	0	0	0	0
19	1375.75	0	0	0	0	0	0	1	0	0	0	0	3	0	0	0	0	0	0	100	0	0	0	0
20	1381.47	0	0	0	0	0	0	0	0	0	0	0	0	0	0	0	0	0	0	0	100	0	0	0
21	1387.15	0	0	0	0	0	0	0	0	0	0	0	0	0	0	0	0	0	0	0	0	100	0	0
22	1415.87	0	0	0	0	0	0	1	0	0	0	0	-1	0	0	0	0	0	0	0	0	0	100	0
23	1422.53	0	0	0	0	0	-1	0	0	0	0	0	0	-4	0	1	0	2	0	0	0	0	0	100

4.4.3 Further Results of the Mode Consolidation Exercise

General consistency and integrity of the present mode consolidated methodology are further indicated in a comparison of various results for the perturbed shell structure below in Table 4.6.

Table 4.6. Comparison of Various Modal Approximations for the Perturbed Shell Structure

Baseline (O)		Perturbed (P)		Consolidated (C)		Modified Guyan Reduction (MGR)			Harmonic Reduction (HR)		
Mode	Freq (Hz)	Mode	Freq (Hz)	Mode	Freq (Hz)	Mode	Freq (Hz)	COR	Mode	Freq (Hz)	COR
1	122.20	1	120.97	1	120.97	1	121.02	100	1	121.02	100
2	122.20	2	121.13	2	121.13	2	121.14	100	2	121.13	100
11	315.24	11	312.43	3	312.43	3	312.38	100	3	312.38	100
14	377.21	15	374.65	4	373.36	4	373.37	100	4	373.35	100
15	377.21	14	373.97	5	374.14	5	374.19	100	5	374.17	100
24	467.77	24	463.45	6	463.45	6	463.50	100	6	463.50	100
49	706.65	48	695.39	7	699.42	7	698.99	100	7	698.99	100
50	706.65	50	701.56	8	701.56	8	701.74	100	8	701.70	100
63	841.31	62	833.52	9	833.71	9	833.72	100	9	833.72	100
76	997.48	76	986.08	10	983.97	10	983.00	100	10	984.52	100
77	997.50	78	994.38	11	994.07	11	994.38	100	11	995.48	100
86	1029.94	85	1020.38	12	1020.02	12	1020.47	100	12	1021.74	100
103	1169.56	101	1149.73	13	1149.62	13	1151.88	100	13	1156.45	100
104	1169.59	104	1166.38	14	1166.38	14	1166.83	100	14	1170.61	100
111	1223.46	108	1200.07	15	1210.08	15	1205.31	99	15	1215.82	99
112	1223.49	112	1219.50	16	1219.59	16	1220.14	100	16	1228.84	100
121	1273.43	123	1266.47	17	1260.33	17	1261.37	99	17	1268.71	99
128	1368.34	131	1363.11	18	1359.92	18	1344.84	94	18	1371.89	91
129	1368.41	132	1366.26	19	1375.75	20	1379.78	84	19	1391.51	80
140	1402.79	136	1373.70	20	1381.47	19	1367.05	76	20	1391.78	74
141	1402.83	142	1402.03	21	1387.15	21	1403.83	76	21	1415.61	74
146	1440.38	147	1433.20	22	1415.87	23	1427.86	78	23	1453.68	82
149	1452.66	144	1419.64	23	1422.53	22	1426.94	88	22	1453.35	9

(O) = Baseline System Body Modes
(P) = Perturbed System Body-Dominant Modes (p=1)
(C) = Perturbed System Consolidated Body Modes (Reference)
(MGR) = Modified Guyan Reduction (Perturbed System)
(HR) = Harmonic Reduction (Perturbed System)

Cross-Orthogonality (COR) : Reference Modes=Consolidated (C)
Reference Mass = Baseline [MFF]

The above results lead to the following observations for the perturbed shell structure:

1. The body dominant modes are remarkably insensitive to introduction of the "line mass" perturbation. This suggests that "features" and "imperfections" in a real structure's make-up may not significantly alter its "body dominant" modes (which are perhaps a reasonable target mode set for practical V&V).
2. Deviation of the last six "body dominant" modal frequencies among the various approximations (especially Consolidated vs. MGR) may be a symptom of truncation in the mode consolidation process, which employs modes up to 1500 Hz; a more authentic consolidation in this range may require inclusion of some modes above 1500 Hz.
3. Modified Guyan Reduction (MGR) appears to be slightly more accurate than Harmonic Reduction (HR).
4. While mixed body and breathing modes for a shell structure are generally unavoidable, mode consolidation may offer an efficient and effective alternative for test mode "comprehension".
5. Moreover, employment of body mode consolidation and MGR may produce an abbreviated, more direct path for test-analysis reconciliation (V&V), which avoids complexities and sensitivities inherent in shell breathing modes.

4.5 Conclusions

Thin shell structures have many breathing modes interspersed among fewer overall body dominant lateral (bending), torsion, and axial-bulge dominant modes within the typically accepted 0-60 Hz frequency band for full-scale launch vehicles. Due to high sensitivity of body (especially bending) modes to configuration features and imperfections (and static pressure and "g" loads), body dominant "target modes" often adopt mixed body-shell breathing (and local appendage) characteristics, which are difficult to discern and verify. Review, comprehension, and categorization of system modes should be treated using two distinct strategies for FEM predictions and experimental modal data, respectively. Modified Guyan Reduction (MGR) and Harmonic Reduction (HR) represent two related options for estimation of body modes (not requiring consolidation operations) for the system FEM. The newly introduced Mode Consolidation (MC) procedure, in contrast, appears to resolve the often noticed "repeated body mode" phenomenon occurring in experimental modal analysis of thin-walled shell structures. It is anticipated that Mode Consolidation will gradually gain acceptance in the technical community as a result of its application in modal testing and inevitable refinements of the strategy.

4.6 References

[1] “Modal Surveys of Weakly Coupled Systems”, A. Klosterman, SAE Technical Paper 760876, 1976

[2] “A Numerically Efficient Finite Element Hydroelastic Analysis”, R. Coppolino, NASA CR-2662, 1976

[3] “DOF Reduction Strategy for Large Order Finite Element Models”, R. Coppolino, IMAC XXIX, 2011

[4] “Automated Response DOF Selection for Mapping of Experimental Normal Modes”, R. Coppolino, IMAC XVI, 1998

[5] “An Automated Method for Identification of Efficient Measurement Degrees-of-Freedom for Mode Survey Testing”, R. Tuttle, T. Cole, and J. Lollock, AIAA 2005-2344, 2005

[6] “Reduction of Stiffness and Mass Matrices”, R. Guyan, AIAA Journal, Vol. 3, No 2, 1965

[7] “Understanding Large Order Finite Element Model Dynamic Characteristics”, R. Coppolino, IMAC XXIX, 2011

[8] “Response DOF Selection for Mapping Experimental Normal Modes-2016 Update”, R. Coppolino, IMAC XXXV, 2016

4.7 Acknowledgments

The Modified Guyan Reduction concept was strongly influenced by conversations, during the mid 1980s, with Robert T. Lahey, who had previously developed and applied a load patch procedure at Lockheed Aircraft Company. Dr. Sheldon Rubin, formerly with The Aerospace Corporation, studied weak coupling in launch vehicle structures over many years since the mid 1970’s. Rubin’s personal notes, under the same title as this paper, followed a different line of thought focusing on launch vehicle flight data based on sparsely allocated instrumentation. It is unfortunate that both Lahey’s and Rubin’s key contributions in model order reduction and mode consolidation, respectively, have not been published in the open literature.

5.0 Part 3: Experimental Mode Verification

5.1 Introduction

Challenges encountered by NASA/MSFC employing the B&K Reflex system for the ISPE modal survey in the Fall of 2016 bring an important challenge to the forefront. The basic question is, "Which estimated test modes are valid, and which modes are questionable or invalid?" This is a multifaceted question that goes well beyond a "knee-jerk" reaction that questions integrity of the B&K Reflex system; it is a question that should apply in virtually all modal test situations. The present discussion on experimental mode verification (EMV) is the result of an ongoing dialogue with Kevin Napolitano of ATA, who pointed out similarities of this writer's idea with Randy Mayes' thoughts[1]. While the presently discussed EMV approach ought to be quite independent of the investigator's choice of a modal extraction algorithm, the results herein apply to methods that explicitly estimate the tested system's "plant" matrix such as the Simultaneous Frequency Domain (SFD) method[2-4].

5.2 Preliminary Thoughts

Consider a structural dynamic system subjected to an applied excitation,

$$[M]\{\ddot{u}\}+[B]\{\dot{u}\}+[K]\{u\}=[\Gamma]\{F\}. \tag{1}$$

On the assumption that the real eigenvectors of the undamped system ([B]=[0]) represent a reasonable set of system modes,

$\{u\}=[\Phi]\{q\}$, where the diagonal modal matrices are (noting $\omega = 2\pi f$, $\omega_n = 2\pi f_n$) (2)

$$[\Phi^T M][\Phi]=[I],\ [\Phi^T K\Phi]=[\omega_n^2],\ [\Phi^T B\Phi]\approx[2\zeta_n\omega_n]. \tag{3}$$

The uncoupled modal acceleration frequency responses are therefore,

$$\ddot{q}(f)=h_n(f)=\frac{-(f/f_n)^2}{1-(f/f_n)^2+2i\zeta_n(f/f_n)}\left(\Phi_n^T\Gamma\right) \tag{4}$$

Finally, the relationship between physical and modal frequency response functions is

$[\ddot{u}(f)]=[H(f)]=[\Phi][h(f)]$, where [h(f)] is the array of modal frequency responses. (5)

If the physical frequency responses, [H(f)], and modal vectors, [Φ], are "known" based on experimental modal analysis, then the uncoupled modal responses, [h(f)], may be estimated by manipulation of equation 5, specifically

$$[h(f)]=[\Phi]^{-1}[H(f)]. \tag{6}$$

Since a truncated set of modes are typically estimated in experimental modal analysis, there are two options for computation of the result in equation 40, namely, (a) exploitation of the mass-weighted modal orthogonality relationship on equation 3), and (b) estimation of $[\Phi]^{-1}$ as the Moor-Penrose pseudo-inverse of [Φ]. The first option is theoretically exact, i.e.,

$$[h(f)]=[\Phi^T M][H(f)]. \tag{7}$$

Accuracy of the above expression requires employment of the TAM mass matrix for [M], which is a subjective estimate, and it is desired that the estimate for $[\Phi]^{-1}$ should not by contingent on model accuracy (evaluation of experimental modal analysis results should initially, at least, be independent of model predictions).

While the second option, which employs the Moore-Penrose pseudo-inverse of [Φ] is independent of model predictions, it can be shown to substantially deviate from the theoretical inverse, [Φ^TM], in many situations. The continuing discussion presented below, addresses this issue for the cases of both real and complex experimental modal vectors.

5.3 The Simultaneous Frequency Domain (SFD) Method

The SFD method[2], introduced in 1981, has undergone substantial revision and refinement since that time[3,4], primarily by this writer and principals at The Aerospace Corporation. SFD implicitly assumes that FRFs associated with multiple excitations relate to a single generalized FRF array as follows:

$$\begin{aligned}&\left[\ddot{U}_1(f)\right]=\left[H_1(f)\right]=\left[V_{1G}\right]\left[H_G(f)\right] \quad \text{(Excitation \#1)}\\ &\left[\ddot{U}_N(f)\right]=\left[H_N(f)\right]=\left[V_{NG}\right]\left[H_G(f)\right] \quad \text{(Excitation \#N).}\end{aligned} \tag{8}$$

The collection of all FRF data is then described by,

$$\begin{bmatrix}H_1(f)\\H_2(f)\\...\\H_N(f)\end{bmatrix}=\begin{bmatrix}V_{1G}\\V_{2G}\\...\\V_{NG}\end{bmatrix}\left[H_G(f)\right]\rightarrow\left[H(f)\right]=\left[V_G\right]\left[H_G(f)\right] \tag{9}$$

By performing a singular value decomposition analysis of the FRF collection, [H(f)], a dominant set of generalized trial vectors, [V_G], and generalized FRFs, [H_G(f)], is obtained. Normalization of the SVD calculations is set such that the trial vectors have unit length, i.e.,

$$\left[V_G\right]^T\left[V_G\right]=\left[I\right] \tag{10}$$

Theoretically, the collection of FRF arrays describes the following dynamic system equations associated with the individual applied forces (where the acceleration arrays are the FRFs, [H_1(f)], ...),

$$\begin{aligned}&\left[\ddot{U}_1(f)\right]+\left[M^{-1}B\right]\left[\dot{U}_1(f)\right]+\left[M^{-1}K\right]\left[U_1(f)\right]=\left[M^{-1}\Gamma_1\right]\left[F(f)\right]\\ &\left[\ddot{U}_2(f)\right]+\left[M^{-1}B\right]\left[\dot{U}_2(f)\right]+\left[M^{-1}K\right]\left[U_2(f)\right]=\left[M^{-1}\Gamma_2\right]\left[F(f)\right]\\ &\left[\ddot{U}_N(f)\right]+\left[M^{-1}B\right]\left[\dot{U}_N(f)\right]+\left[M^{-1}K\right]\left[U_N(f)\right]=\left[M^{-1}\Gamma_N\right]\left[F(f)\right].\end{aligned} \tag{11}$$

The physical velocity and displacement arrays are successively formed by "2iπf" division. By noting that the force array associated with each FRF array is a "unit" row matrix, the collection of all frequency response data is expressed as,

$$\begin{bmatrix}\ddot{U}_1(f)\\...\\\ddot{U}_N(f)\end{bmatrix}+\left[M^{-1}B\right]\begin{bmatrix}\dot{U}_1(f)\\...\\\dot{U}_N(f)\end{bmatrix}+\left[M^{-1}K\right]\begin{bmatrix}U_1(f)\\...\\U_N(f)\end{bmatrix}=\begin{bmatrix}M^{-1}\Gamma_1\\...\\M^{-1}\Gamma_N\end{bmatrix}\left[F(f)\right]. \tag{12}$$

Introducing the SVD-based reduction transformation (equation 9),

$$\begin{bmatrix}\ddot{U}_1(f)\\...\\\ddot{U}_N(f)\end{bmatrix}=\begin{bmatrix}V_{1G}\\...\\V_{NG}\end{bmatrix}\left[\ddot{\xi}(f)\right]=\left[V_G\right]\left[\ddot{\xi}(f)\right], \text{ etc. for velocity and displacement,} \tag{13}$$

the following effective dynamic system is defined,

$$\left[V_G^T V_G\right]\left[\ddot{\xi}(f)\right]+\left[V_G^T\left[M^{-1}B\right]V_G\right]\left[\dot{\xi}(f)\right]+\left[V_G^T\left[M^{-1}K\right]V_G\right]\left[\xi(f)\right]=\left[V_G^T\right]\begin{bmatrix} M^{-1}\Gamma_1 \\ ... \\ M^{-1}\Gamma_N \end{bmatrix}\left[F(f)\right], \text{ or}$$

$$\left[\ddot{\xi}(f)\right]+\left[\tilde{B}\right]\left[\dot{\xi}(f)\right]+\left[\tilde{K}\right]\left[\xi(f)\right]=\left[\tilde{\Gamma}\right]\left[F(f)\right]. \tag{14}$$

Note that "$M^{-1}B$" and "$M^{-1}K$" partitions in the above equation set represent the "repeat-chain" coefficient matrices in equation13. Before proceeding further in this derivation, it should be noted that the above effective dynamic system (with unit applied "row" force array, [F(f)]), collects all applied excitation force-based FRF data into a single generalized, effective dynamic system. Moreover, the reader is reminded that the generalized accelerations are actually the generalized FRFs, $[H_G(f)]$, that were formed in the FRF SVD calculations (equations 8-10). And, as in the case of physical FRF data, the generalized velocity and displacement arrays are successively formed by "$2i\pi f$" division. An important feature of the effective dynamic system, defined by equation 14, is that it represents system response to all excitations simultaneously. This attribute maximizes the opportunity to automatically account for very closely-spaced and/or repeated (same eigenvalue) modes.

The matrices associated with the effective dynamic system are estimated through linear least squares analysis of the following equation set (where [R] represents the "residual" error):

$$\left[\ddot{\xi}(f)\right]=\left[-\tilde{B}\quad -\tilde{K}\quad \tilde{\Gamma}\right]\begin{bmatrix}\dot{\xi}(f)\\ \xi(f)\\ F(f)\end{bmatrix}+\left[R\right]$$

$$\left[-\tilde{B}\quad -\tilde{K}\quad \tilde{\Gamma}\right]=\left(\left[\ddot{\xi}(f)\right]\cdot\begin{bmatrix}\dot{\xi}(f)\\ \xi(f)\\ F(f)\end{bmatrix}^T\right)\cdot\left(\left(\begin{bmatrix}\dot{\xi}(f)\\ \xi(f)\\ F(f)\end{bmatrix}\cdot\begin{bmatrix}\dot{\xi}(f)\\ \xi(f)\\ F(f)\end{bmatrix}^T\right)^{-1}\right) \tag{15}$$

It should be noted that, due to the fact that the generalized FRF arrays are complex, actual details of the least-squares estimation computations are more involved than implied by the above relationships.

Estimation of experimental modal parameters is performed by complex eigenvalue analysis of the state variable form of the effective dynamic system,

$$\begin{Bmatrix}\ddot{\xi}\\ \dot{\xi}\end{Bmatrix}=\begin{bmatrix}-\tilde{B} & -\tilde{K}\\ I & 0\end{bmatrix}\begin{Bmatrix}\dot{\xi}\\ \xi\end{Bmatrix}+\begin{bmatrix}\tilde{\Gamma}\\ 0\end{bmatrix}\{F\}, \text{ which is of the general type, } \{\dot{\eta}\}=\left[A_\eta\right]\{\eta\}+\left[\Gamma_\eta\right]\{F\} \tag{16}$$

Complex eigenvalue analysis of the effective dynamic system produces the following results:

(a) $\{\eta\}=\left[\Phi_\eta\right]\{q\}$ where the "left-handed" eigenvectors are $\left[\Phi_{\eta L}\right]=\left[\Phi_\eta\right]^{-1}$

(b) $\left[\Phi_{\eta L}\right]\cdot\left[\Phi_\eta\right]=\left[I\right]$, $\left[\Phi_{\eta L}\right]\cdot\left[A_\eta\right]\left[\Phi_\eta\right]=\left[\lambda\right]$ (complex eigenvalues)

(c) $\left[\Phi_{\eta L}\right]\cdot\left[\Gamma_\eta\right]=\left[\gamma\right]$ (modal gains) (17)

(d) $\dot{q}_j-\lambda_j q_j=(\gamma)_j F(f)$ (frequency response of individual modes).

Recovery of experimental modes in terms of the physical DOFs involves back transformation employing the trial vector matrix, $[V_G]$.

5.4 Selection of Valid Experimental Modal Data (the Heart of the Present Discussion)

Estimation of the effective dynamic system with the SFD method (and more generally any method that performs similar system "plant" estimation operations) will pick up spurious "noise" degrees of freedom and associated spurious modes. Over the years since 1981, the writer has employed a heuristic practice in versions of SFD algorithms that select "valid" modes from the complete set, which is estimated in selected frequency bands. The heuristic criteria include, (1) elimination of modes having negative damping, (2) modes with very low modal gain, and (3) other modes that appear spurious from any number of physical/experience based considerations. The present discussion is a radical departure from past practice in that it endeavors to replace heuristic criteria with a more rigorous criterion.

The initial point of departure from past SFD practice is estimation of an effective dynamic system over the entire frequency band of interest (in the case of ISPE, the range is 0-60 Hz). In order to achieve a satisfactory estimation for the effective dynamic system, the "tolerance" factor employed in the SVD process described by equations 8-10 is set to a sufficiently low value (10^{-5}); in previous "band-limited" SFD calculations, the SVD "tolerance" factor was set to a value of 10^{-2}.

Computation of effective dynamic system modal parameters, from the first-order system described in equation 16, yields complex modes with eigenvalues having negative and positive real parts. The first level of mode down-selection is to eliminate all modal eigenvalues and eigenvectors that are outside the frequency band of interest. For the ISPE modal test, there are 133 complex eigenvalues in the 15-60 Hz frequency band. A vital component of the mode down-selection process is selection of left-hand eigenvectors. $[\Phi_{\eta L}]$ that correspond to their $[\Phi_{\eta}]$ counterparts; this circumvents issues associated with more involves procedures for computation of a truncated left-hand eigenvector set.

There are two computational procedures to estimate uncoupled experimental modal FRFs. The first method computes the exact modal solution from the estimated modal parameters of equation 17d. Specifically,

$$\left[h_j(f)\right]_{mod} = \dot{\eta} = \left(\frac{i2\pi f}{i2\pi f - \lambda_j}\right)\gamma_j \tag{18}$$

The second method estimates uncoupled experimental modal FRFs from linear combinations of the generalized FRFs, $[H_G(f)]$, as follows:

$$\left[h_j(f)\right]_G = \dot{\eta}_G = \left[\Phi_{\eta L}\right]_j \cdot \begin{bmatrix} \ddot{\xi}(f) \\ \dot{\xi}(f) \end{bmatrix} = \left[\Phi_{\eta L}\right]_j \cdot \begin{bmatrix} H_G(f) \\ H_G(f)/(i2\pi f) \end{bmatrix} \tag{19}$$

Verification (selection and validation) of any candidate estimated experimental mode is now to be judged on the basis of (a) graphical displays of the modal FRFs, and (b) a new modal coherence metric, which is defined as,

$$COH_j = \frac{\left|\left[h_j(f)\right]^*_{mod} \cdot \left[h_j(f)\right]_G\right|^2}{\left|\left[h_j(f)\right]^*_{mod} \cdot \left[h_j(f)\right]_{mod}\right| \cdot \left|\left[h_j(f)\right]^*_G \cdot \left[h_j(f)\right]_G\right|} \tag{20}$$

In addition, (c) a third, potential weaker selection metric is the magnitude and phase of the modal gain, γ_j, defined in equation 17c.

5.4.1 ISPE Experimental Mode Verification (EMV)

While detailed results of ISPE EMV are presented in Appendix E, typical results of that exercise are provided in this section.

Modal FRFs for the first seven candidate modes are illustrated in the following seven figures (Figure 5.1 through Figure 5.7) the include FRF magnitude, magnitude and phase, polar, and real and imaginary parts.

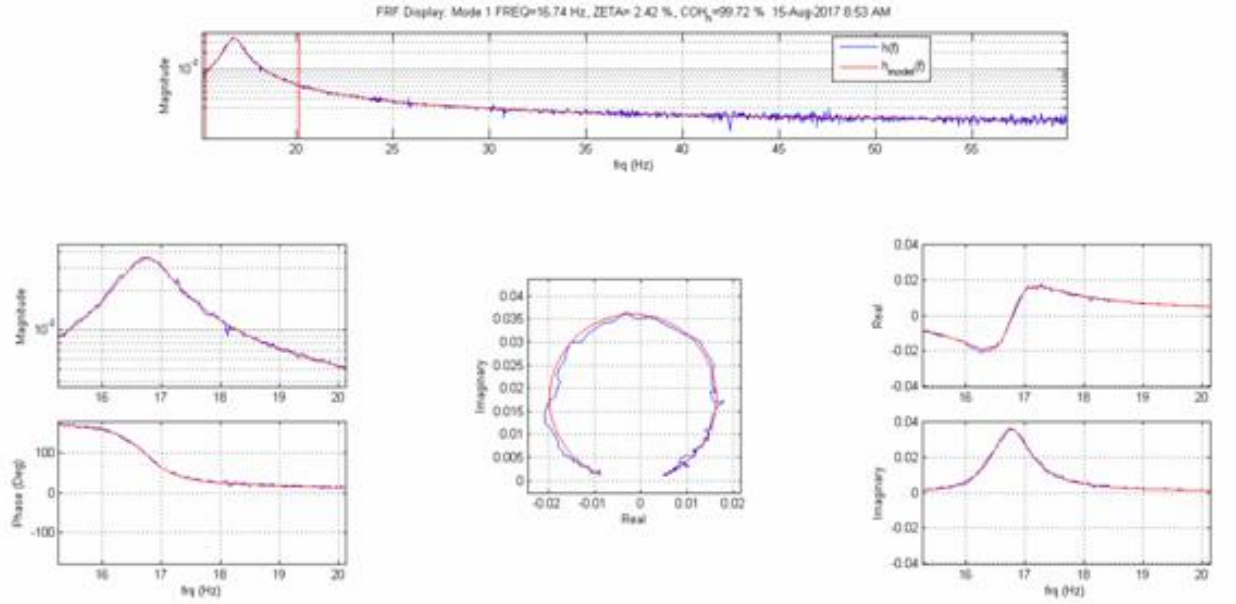

Figure 5.1. EMV Graphic for ISPE Candidate Mode 1, 16.74 Hz

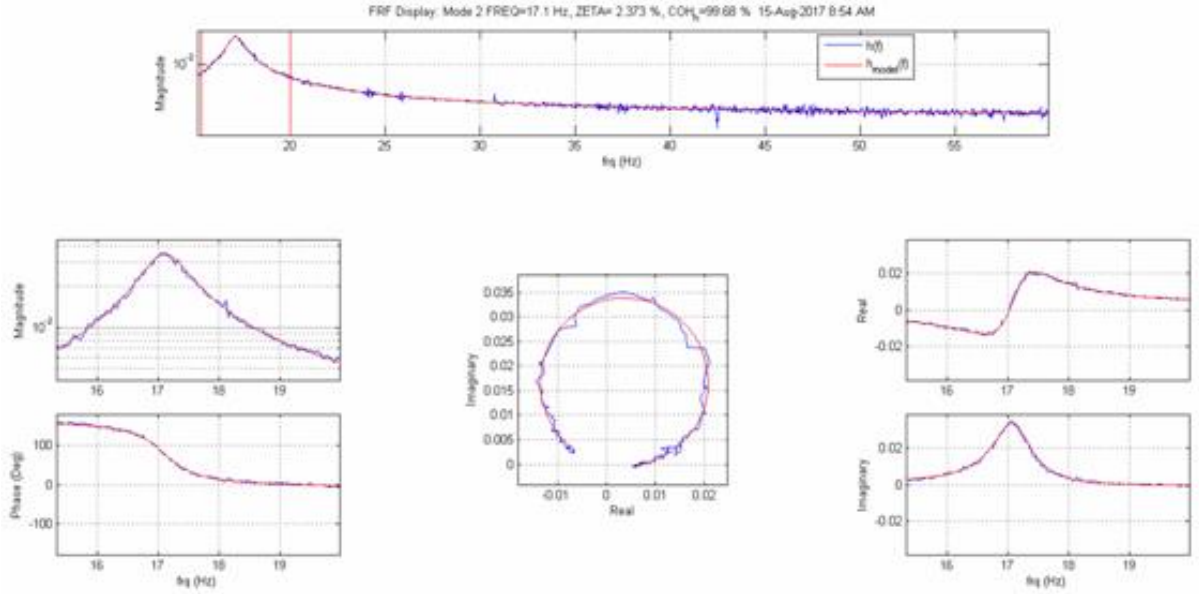

Figure 5.2. EMV Graphic for ISPE Candidate Mode 2, 17.10 Hz

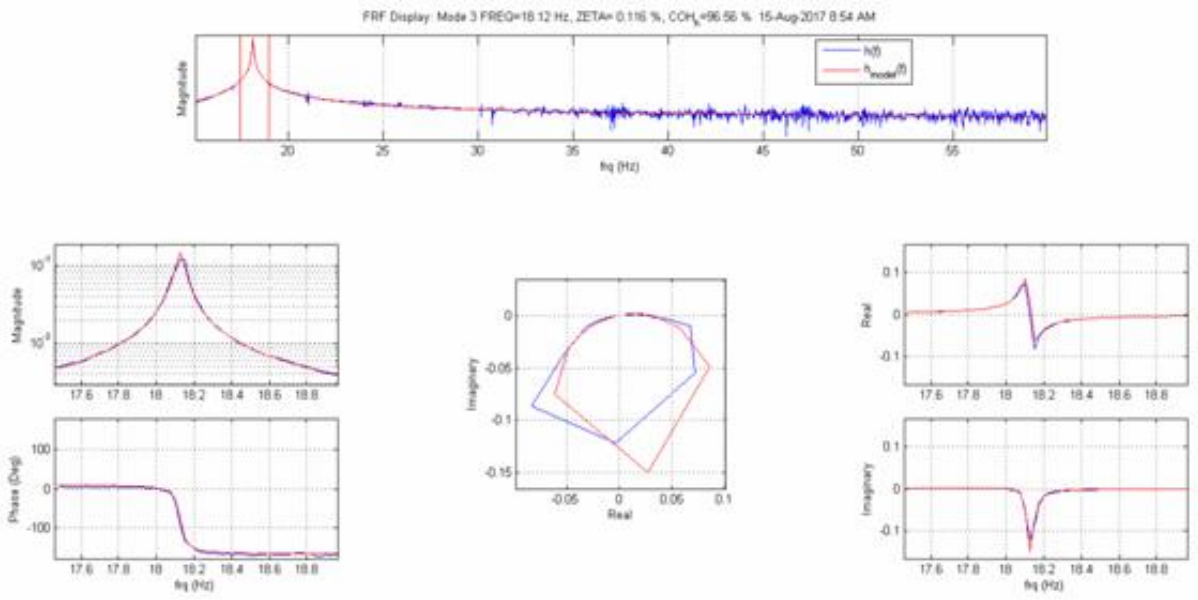

Figure 5.3. EMV Graphic for ISPE Candidate Mode 3, 18.12 Hz

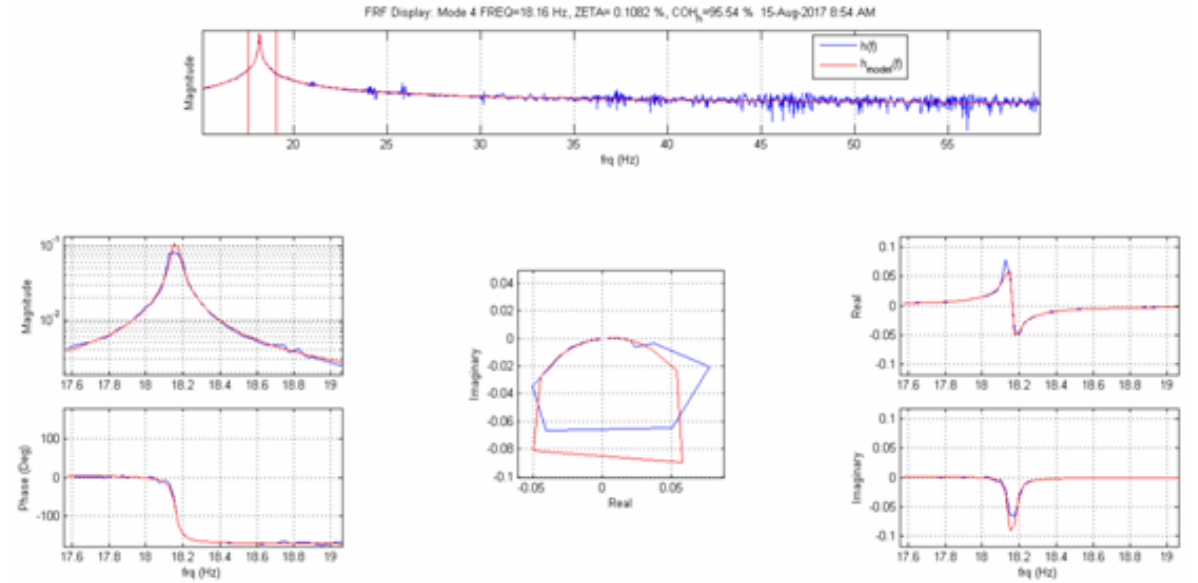

Figure 5.4. EMV Graphic for ISPE Candidate Mode 4, 18.16 Hz

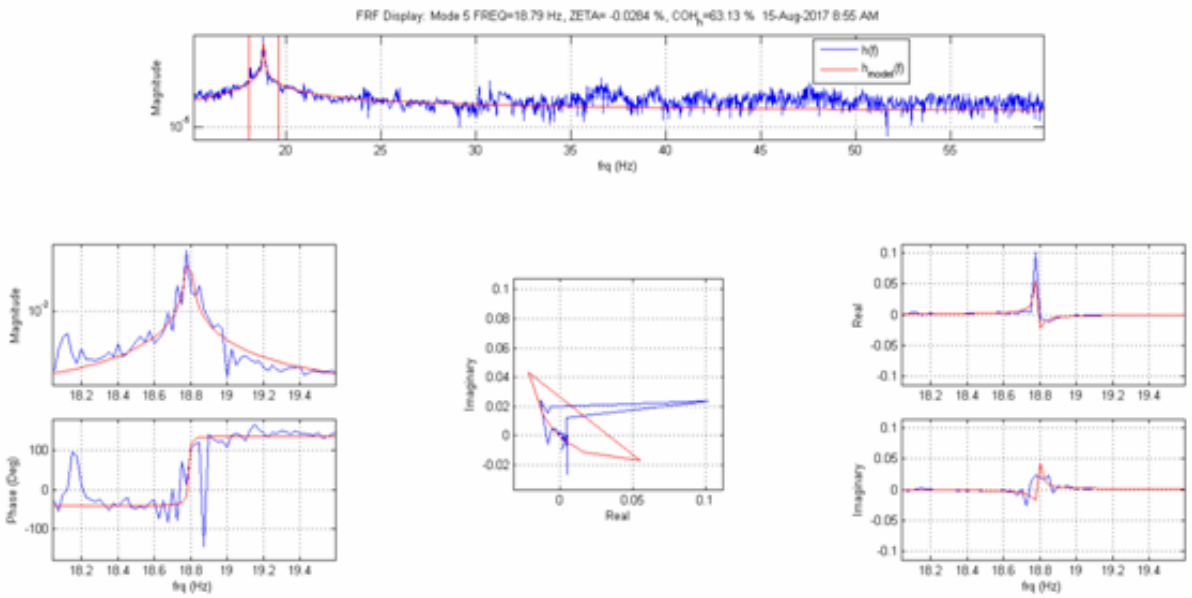

Figure 5.5. EMV Graphic for ISPE Candidate Mode 5, 18.79 Hz

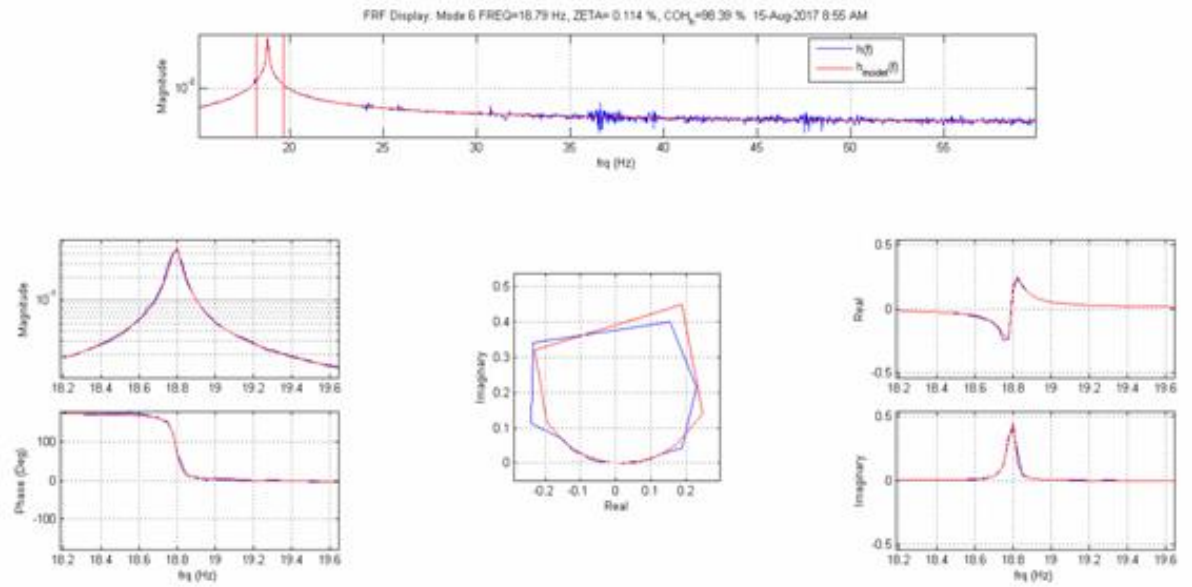

Figure 5.6. EMV Graphic for ISPE Candidate Mode 6, 18.79 Hz

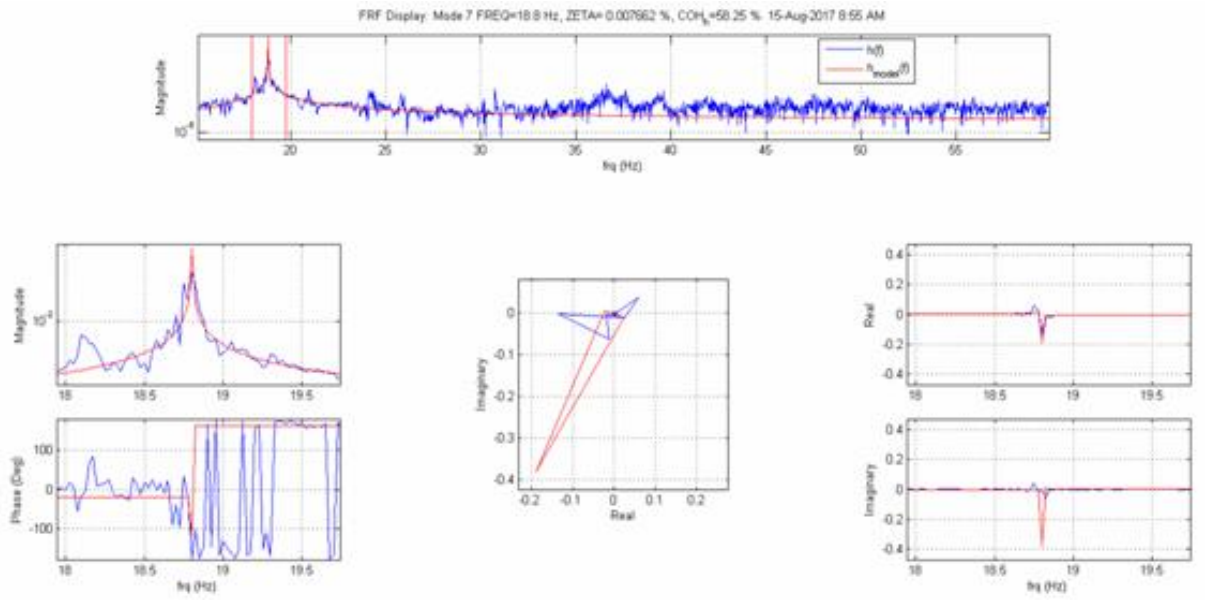

Figure 5.7. EMV Graphic for ISPE Candidate Mode 7, 18.80 Hz

It is clear in the above seven figures that candidate modes 1-4 and 6 appear valid based on close agreement of the two types of uncoupled modal FRF estimates. In contrast, candidate modes 5 and 7 appear to be spurious and invalid.

A complete, numerical EMV assessment for the 133 candidate ISPE experimental modes is summarized in Tables 5.1 through 5.3, which are self explanatory in content.

Table 5.1. EMV for ISPE Candidate Modes 1-45

EV	Eigenvalue		Excitation (PHIL*GAM)		Evaluation Critera & Assessment		
	FREQ (Hz)	Zeta (%)	|Gain| (%)	Phase (deg)	max|h| (%)	Coherence (%)	Is it a mode?
1	16.74	2.42	9	6.9	2.11	100	Y
2	17.10	2.37	8	-11.0	2.04	100	Y
3	18.13	0.12	2	-169.2	6.99	97	Y
4	18.16	0.11	1	-174.2	4.72	96	Y
5	18.79	-0.03	0	137.5	6.00	63	N
6	18.79	0.11	6	-4.0	24.72	98	Y
7	18.80	0.01	0	161.1	7.71	58	N
8	19.28	0.08	1	-2.6	2.31	88	Y
9	20.36	2.81	6	165.7	1.31	99	Y
10	20.90	0.03	0	-118.2	4.25	18	N
11	20.96	0.07	2	-8.9	10.86	88	Y?
12	21.02	0.07	2	156.2	11.47	91	Y?
13	21.25	0.05	1	163.7	1.72	2	N
14	22.43	-2.12	1	13.0	0.86	4	N
15	24.02	0.10	1	-2.1	2.44	86	Y?
16	24.07	0.46	12	-175.5	15.21	100	Y
17	24.27	0.44	12	175.0	15.52	100	Y
18	25.82	0.14	4	4.5	13.89	100	Y
19	25.88	-0.01	0	-58.7	2.99	10	N
20	25.89	0.12	4	-0.2	16.30	99	Y
21	26.75	-0.85	1	153.8	0.50	1	N
22	27.53	1.65	7	26.3	2.66	100	Y
23	27.81	1.54	9	159.8	3.15	100	Y
24	28.41	-0.34	0	67.2	0.43	0	N
25	30.14	-0.01	1	138.7	4.35	8	N
26	30.15	0.33	2	-167.1	3.31	62	Y?
27	31.00	-0.83	1	61.0	1.33	2	N
28	31.78	-0.43	1	-55.8	0.63	0	N
29	32.32	1.08	3	-163.5	1.31	95	Y?
30	33.15	1.03	7	80.9	3.46	95	N
31	33.42	0.32	5	-113.0	8.72	96	Y?
32	33.70	-0.07	1	-59.3	1.66	0	N
33	34.18	2.23	20	148.4	5.00	100	Y
34	34.22	0.03	0	-116.1	0.51	3	N
35	34.64	-0.23	0	-101.3	0.44	0	N
36	35.42	0.53	10	-165.1	8.94	99	Y
37	35.77	-10.73	7	72.0	0.68	32	N
38	35.96	-0.23	1	106.1	1.57	1	N
39	35.97	1.16	12	157.8	6.04	100	Y
40	36.21	0.14	5	163.3	18.03	98	Y
41	36.30	0.09	1	13.2	4.01	67	N
42	36.47	0.31	54	137.4	99.69	100	Y
43	36.51	0.00	0	-151.1	2.74	28	N
44	36.55	-0.05	0	103.5	4.34	1	N
45	36.61	0.56	100	-159.1	100.00	100	Y

Table 5.2. EMV for ISPE Candidate Modes 45-90

EV	Eigenvalue		Excitation (PHIL*GAM)		Evaluation Critera & Assessment		
	FREQ (Hz)	Zeta (%)	|Gain| (%)	Phase (deg)	max|h| (%)	Coherence (%)	Is it a mode?
46	36.76	-0.07	0	45.4	1.34	3	N
47	36.92	0.17	2	109.1	4.65	73	N
48	37.03	0.25	7	8.1	16.80	99	Y?
49	37.24	-0.13	1	-70.8	3.68	0	N
50	37.27	0.47	18	-101.4	22.79	99	Y?
51	37.36	0.30	20	-161.4	36.59	100	Y
52	37.69	0.36	19	158.1	30.11	100	Y
53	37.99	-0.07	0	24.2	1.06	0	N
54	38.13	0.09	1	-15.9	1.13	20	N
55	38.30	1.22	17	-57.8	7.97	99	Y
56	38.55	-0.09	1	-65.5	0.92	0	N
57	38.71	0.04	0	160.9	1.85	23	N
58	38.81	0.12	2	13.2	4.98	62	N
59	38.92	2.14	37	-77.3	10.35	99	Y
60	39.35	-0.41	1	103.4	0.83	1	N
61	39.41	0.62	18	-38.9	15.34	99	Y?
62	39.54	0.16	4	-161.5	14.33	98	Y?
63	39.68	0.70	15	-80.4	12.27	96	Y?
64	39.90	0.31	2	115.1	2.46	58	N
65	40.40	-0.03	0	-0.5	0.40	0	N
66	40.99	0.03	0	86.9	1.85	8	N
67	41.18	-0.98	4	-129.2	2.61	2	N
68	41.22	-0.17	1	8.1	1.84	0	N
69	41.71	0.78	46	166.6	32.62	99	Y
70	41.88	0.04	4	73.0	8.51	31	N
71	42.02	0.95	36	22.2	22.07	99	Y
72	42.57	0.03	0	-42.6	0.64	3	N
73	42.93	0.01	1	-46.7	0.78	1	N
74	43.11	-0.01	0	-35.1	1.00	0	N
75	43.45	0.99	92	-2.3	52.01	100	Y
76	43.51	-8.62	11	-43.5	1.83	32	N
77	43.63	0.03	1	55.5	1.56	16	N
78	43.73	0.49	8	148.6	8.23	98	Y?
79	43.98	0.08	1	152.6	1.63	33	N
80	44.49	-0.14	1	-15.3	0.70	0	N
81	44.70	0.04	1	17.5	2.61	12	N
82	45.00	0.39	10	178.3	13.83	99	Y
83	45.02	0.04	1	-97.9	4.04	41	N
84	45.35	-0.10	1	-178.5	1.77	0	N
85	45.54	0.15	2	-17.5	8.13	90	Y?
86	45.72	2.10	49	-158.7	13.36	100	Y
87	45.77	0.00	0	-64.1	2.20	2	N
88	45.87	-0.96	3	46.2	2.24	2	N
89	45.92	0.05	1	-159.1	5.97	15	N
90	46.11	0.00	0	-9.3	38.44	22	N

Table 5.3. EMV for ISPE Candidate Modes 91-133

EV	Eigenvalue		Excitation (PHIL*GAM)		Evaluation Critera & Assessment		
	FREQ (Hz)	Zeta (%)	|Gain| (%)	Phase (deg)	max|h| (%)	Coherence (%)	Is it a mode?
91	46.15	-0.01	1	-115.3	44.25	76	N
92	46.24	0.13	4	-142.3	13.66	52	N
93	46.49	0.50	18	81.7	21.27	99	Y
94	46.65	0.76	49	175.6	36.27	100	Y
95	46.96	-0.01	0	-166.0	4.44	2	N
96	46.98	0.23	6	59.8	12.55	91	N
97	47.48	0.22	7	-135.1	17.45	99	Y
98	47.62	0.83	64	-30.8	44.04	100	Y
99	47.78	-0.23	1	75.0	1.43	0	N
100	47.83	0.37	7	-8.8	10.03	98	Y?
101	48.11	1.54	56	15.4	21.03	100	Y
102	48.38	0.24	3	-99.5	4.45	86	N
103	48.58	-0.04	0	161.7	1.04	0	N
104	48.89	-0.11	1	135.8	1.11	0	N
105	49.18	0.75	20	-26.6	14.84	100	Y
106	50.05	0.75	11	-141.6	8.99	99	Y?
107	50.20	0.10	1	-19.4	2.30	53	N
108	50.44	0.33	6	85.7	9.16	97	Y?
109	50.69	0.18	3	141.2	6.82	91	N?
110	50.93	0.49	16	156.3	17.32	99	Y?
111	51.26	0.19	3	69.0	7.05	85	N
112	51.32	0.48	23	33.8	25.71	99	Y
113	51.45	1.47	56	-178.8	21.49	100	Y
114	52.28	0.03	0	67.6	1.33	4	N
115	52.73	-0.07	1	30.4	0.99	0	N
116	53.43	0.57	12	79.8	12.76	99	Y?
117	53.62	1.64	54	3.4	18.42	100	Y
118	53.80	0.23	5	58.8	9.09	96	Y?
119	54.18	0.01	3	169.1	5.52	10	N
120	54.32	0.52	15	-115.7	15.63	99	Y?
121	55.11	-0.39	1	-31.7	1.00	1	N
122	55.26	1.04	44	15.3	23.55	100	Y
123	55.44	0.62	19	-26.6	16.11	99	Y
124	55.99	0.00	1	82.6	1.24	1	N
125	56.38	0.58	13	-149.9	12.06	99	Y
126	57.33	0.93	30	142.0	18.25	100	Y
127	57.88	0.36	6	-157.6	8.80	98	Y
128	58.03	-0.03	0	68.5	1.66	0	N
129	58.40	0.38	11	143.9	15.37	99	Y
130	58.56	1.25	64	12.5	28.51	100	Y
131	58.77	0.09	1	-22.1	5.50	59	N
132	59.43	0.02	1	61.9	4.76	26	N
133	59.65	0.13	4	-154.0	13.25	96	Y?

The above tabular summaries provide a clear demonstration of the utility of the newly introduced EMV metrics (particularly the modal coherence metric defined in equation 20 for which a value of 95% or greater generally indicates a validly estimated mode).

5.4.2 Estimation of Experimental Modal Vectors

Once a valid set of experimental eigenvalues are selected, the associated eigenvectors (modal vectors) must be estimated. There are three distinct approaches for estimation of, namely,

(a) Employment of the SFD vector transformations, $[V_G]$ and $[\Phi_\eta]$
(b) Global linear least squares fit of complex modal vectors
(c) Global linear least squares fit of real modal vectors.

The first approach estimates the complex modal vectors as,

$$[\Phi] = [V_G][\Phi_\eta]_{acc}, \tag{21}$$

where the "acc" subscript refers to the partition of $[\Phi_\eta]$ associated with $\ddot{\xi}$ (see equation 16). This computation is strictly limited to the SFD method.

The second approach performs a linear least squares analysis on the following well-known relationship (in terms of the frequencies $\omega = 2\pi f$),

$$[H(\omega)] = \sum_j \left(\frac{\Phi_j}{\lambda_j - i\omega} + \frac{\Phi_j^*}{\lambda_j^* - i\omega} \right), \tag{22}$$

where $[H(\omega)]$ is the measured FRF array (for all responses and excitations, see equation 9), and $\lambda_j = \sigma_j + i\omega_j$ are the selected estimated complex eigenvalues.

The third approach performs a linear least squares analysis on the following relationship (in terms of the frequencies $\omega = 2\pi f$),

$$[H(\omega)] = [\Phi][h(\omega)], \text{ where} \tag{23}$$

$$h_j(\omega) = \frac{-\omega^2}{\omega_j^2 - \omega^2 + 2i\zeta_j\omega_j\omega}, \text{ for each mode "j".}$$

All three approaches for experimental modal vector estimation have an inherent associated challenge related to the fact that the modal vectors, $[\Phi]$, that is actually a composite of estimates corresponding to the independent excitations (see equations 8-13), i.e.,

$$[\Phi] = \begin{bmatrix} \Phi_1 \\ \dots \\ \Phi_N \end{bmatrix} \text{ associated with excitations } \begin{bmatrix} "F_1" \\ \dots \\ "F_N" \end{bmatrix} \tag{24}$$

Ideally, the modal excitation related partitions for each individual modal vector, $\{\Phi\}$, should be proportional to one another, but this is approximately true or not at all true if there are multiple repeated modes at the same eigenvalue. Resolution of this issue is realized based on a combination of special calculations (e.g., SVD) and the test engineer's judgment and experience.

Finally, it is noted that the prevailing approach employed in V&V relies on real experimental modal vectors. In this context, global linear least squares fitting of real modal vectors is preferred. The alternative approach relates to calculation of "best fit" real mode approximations for estimated complex modal vectors.

5.5 Conclusions

Experimental modal analysis is a very mature discipline in the structural dynamics community, which is as much an "art" as it is a "science". Modern procedures for estimation of modal parameters from measured data are highly automated; however, applications involving complicated structural systems and/or systems with closely-spaced, parametrically sensitive modes require the test engineer's experience and judgment ("art") to discern the difference between authentic and spurious ("junk" or "noise") system modes. A prevailing metric for experimental modal data validation is the orthogonality check, which relies on a model-based (TAM) mass matrix. In addition, reconstructive synthesis of measured frequency

response function (FRF) data is another widely used strategy for experimental mode validation. The present EMV study employs mathematical operations aimed at isolating individual candidate experimental modes without reliance on a TAM mass matrix. In a sense EMV, as presented in this report, recalls past heuristic graphical techniques ("art") for discernment of experimental modes in a formal mathematical ("science") sense.

The key to mathematical and visual isolation of individual modes from measured data is the left-hand eigenvector. Virtually all modern experimental modal analysis techniques produce estimates of right-hand eigenvectors and eigenvalues (modal frequency and damping). While techniques for estimation of left-hand eigenvectors are well-known (e.g., "$[\Phi^T M]$" and the Moore-Penrose pseudo-inverse), they have been judged inadequate during the course of the present study. The purest approach to estimation of left-hand eigenvectors is a consequence of some experimental modal analysis techniques, specifically those techniques that estimate the measured system's plant or effective dynamic system matrix. Since a complete set of (authentic and "junk") system modes are identified for the estimated plant, the left-hand eigenvectors are calculated exactly from the inverse of the complete right-hand eigenvector set.

The following metrics provide a systematic basis for EMV:

(1) The estimated Single-Degree-of-Freedom (SDOF) modal FRF, formed by the product of a single estimated left-hand eigenvector and FRF matrix, is plotted in terms of real and imaginary components vs. frequency, magnitude and phase components vs. frequency, and polar real vs. imaginary components. Authenticity of an estimated mode is then judged on the basis of quality of the plots.

(2) The SDOF modal FRF is also formed from exact mathematical solution of the estimated effective dynamic system. Graphical comparison of this result with the above left-handed product information offers further means of authentic vs. "junk" mode discrimination.

(3) Finally, a coherence metric based on comparison of the results of "1" and "2" provides a 0-to-100% figure of merit for estimated experimental modes.

As a closing thought regarding EMV, it is suspected that estimated left-handed eigenvectors may ultimately provide the means to compute test-analysis cross-orthogonality independent of the TAM mass matrix. This, of course, is the subject of a future endeavor.

5.6 References

[1] "The SMAC Modal Parameter Extraction Package", Mayes and Klenke, IMAC 17, 1999.

[2] "A Simultaneous Frequency Domain Technique for Estimation of Modal Parameters from Measured Data", Coppolino, SAE Paper 811046, 1981

[3] "A Global Technique for Estimation of Modal Parameters from Measured Data" Coppolino and Stroud, SAE Paper 851926, 1985

[4] "Efficient and Enhanced Options for Experimental Mode Identification", Coppolino, IMAC 21, 2003

REPORT DOCUMENTATION PAGE

Form Approved
OMB No. 0704-0188

1. REPORT DATE *(DD-MM-YYYY)*	2. REPORT TYPE	3. DATES COVERED *(From - To)*
01/22/2018	Contractor Report	

4. TITLE AND SUBTITLE
Methodologies for Verification and Validation of Space Launch System (SLS) Structural Dynamic Models

5a. CONTRACT NUMBER
NNL12AA09C

5b. GRANT NUMBER

5c. PROGRAM ELEMENT NUMBER

6. AUTHOR(S)
Coppolino, Robert N.

5d. PROJECT NUMBER

5e. TASK NUMBER

5f. WORK UNIT NUMBER
869021.03.07.01.03

7. PERFORMING ORGANIZATION NAME(S) AND ADDRESS(ES)
NASA Langley Research Center
Hampton, VA 23681-2199

8. PERFORMING ORGANIZATION REPORT NUMBER

9. SPONSORING/MONITORING AGENCY NAME(S) AND ADDRESS(ES)
National Aeronautics and Space Administration
Washington, DC 20546-0001

10. SPONSOR/MONITOR'S ACRONYM(S)
NASA

11. SPONSOR/MONITOR'S REPORT NUMBER(S)
NASA/CR-2018-219800/Vol I

12. DISTRIBUTION/AVAILABILITY STATEMENT
Unclassified - Unlimited
Subject Category 16 Space Transportation and Safety
Availability: NASA STI Program (757) 864-9658

13. SUPPLEMENTARY NOTES
This report was prepared for the NASA Engineering and Safety Center by Measurement Analysis Corporation, Reston, Virginia. under NASA contract number NNL12AA09C.

14. ABSTRACT
Verification and validation (V&V) is a highly challenging undertaking for SLS structural dynamics models due to the magnitude and complexity of SLS subassemblies and subassemblies. Responses to challenges associated with V&V of Space Launch System (SLS) structural dynamics models are presented in this paper. Four methodologies addressing specific requirements for V&V are discussed. (1) Residual Mode Augmentation (RMA). (2) Modified Guyan Reduction (MGR) and Harmonic Reduction (HR, introduced in 1976). (3) Mode Consolidation (MC). Finally, (4) Experimental Mode Verification (EMV).

15. SUBJECT TERMS
Verification and Validation; Space Launch System; Residual Mode Augmentation; Modified Guyan Reduction; Mode Consolidation; Experimental Mode Verification

16. SECURITY CLASSIFICATION OF:			17. LIMITATION OF ABSTRACT	18. NUMBER OF PAGES	19a. NAME OF RESPONSIBLE PERSON
a. REPORT	b. ABSTRACT	c. THIS PAGE			STI Help Desk (email: help@sti.nasa.gov)
					19b. TELEPHONE NUMBER *(Include area code)*
U	U	U	UU	45	(443) 757-5802